SOLVENT INDUCED STRUCTURES IN THIN POLYMER FILMS

A thesis submitted in partial fulfillment
of the requirements for the degree of
Master of Technology

By

SUBHASHIS SARKAR

to the

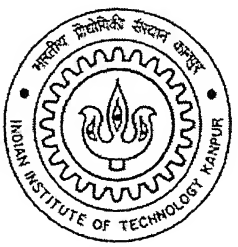

DEPARTMENT OF CHEMICAL ENGINEERING
INDIAN INSTITUTE OF TECHNOLOGY KANPUR
JULY 2004

9-7-04

CERTIFICATE

Certified that the work contained in this thesis entitled – "**SOLVENT INDUCED STRUCTURES IN THIN POLYMER FILMS**", by Subhashis Sarkar, has been carried out under my supervision and that this work has not been submitted elsewhere for a degree.

Dr. Ashutosh Sharma
Professor & Head
Department of Chemical Engineering
Indian Institute of technology
Kanpur 208016

July 2004

Abstract

In most of the previous studies dewetting is induced by heating, i.e. by increasing the temperature above Glass Transition Temperature. We observed that dewetting of thin polymer film can be induced by solvent also. Solvent is introduced in two different ways. Firstly as a liquid solvent layer over the polymer film and secondly, polymer film is exposed in solvent vapour. Dewetting occurred in both the cases and various characteristic patterns are observed.

For the first case depending upon the relative rate of evaporation of solvent and dissolution of polymer in solvent, different patterns are observed. The effect of substrate, polymer film thickness, temperature, Nitrogen flow rate on the pattern formed is studied. Parallel array of polymer dots of micrometer size can be produced by this method. The size of the polymer dots, spacing, and distance between two parallel lines can be altered by changing the various parameters.

When thin (<50nm) polymer film is exposed in solvent atmosphere at room temperature (25°C) the film dewets through formation of holes, hole growth, hole coalescence to form polygonal network structure, which finally disintegrate into polymer droplets. A possible reason for dewetting at temperature well below its Glass transition temperature (~100°C) is proposed and the characteristic features are compared with the present theory of temperature induced dewetting.

Acknowledgements

I would like to express my sincere gratitude to my thesis supervisor Dr. Ashutosh Sharma, for his excellent guidance, encouragement and support throughout the progress of this work. I consider myself very fortunate to work with such a nice person, teacher and guide.

I am especially thankful to Manoj Gonuguntla S for all his help and inputs given in every step of my work. Discussions with him are really helpful.

I take this opportunity to express my thanks to all my lab-mates, especially Moniraj and Ritesh for there true concern about my work. They always stood by my side at hard times.

Thanks to Rabi da, Kasturi and Subramanian for their help.

I pay my sincere gratitude to all my teachers for kindling the light of knowledge and reason in my mind.

I am thankful to all non teaching stuffs especially Mr. R. Vishwakarma for helping me to make the experimental setup.

I am very much thankful to all my friends, Sukalyan, Prakash da, Debu da who made my stay at IIT Kanpur so much fun and memorable.

Finally, I would like to thank my parents and brothers for their love, support and encouragement. Everything I have I owe it to them.

Subhashis Sarkar

Dedicated
to
My Parents

CONTENTS

LIST OF TABLES

LIST OF FIGURES

3.7 Polymer droplets observed in the central region when a 0.7mm thick solvent layer placed over a 50nm film is allowed to evaporate in ambient at a. 25°C and b. 20°C. No density of polymer droplets increases with increasing thickness. Bar size is 10 μm.

3.8 Features observed in the central region when a 0.7mm thick solvent layer placed over a 115nm film is allowed to evaporate in ambient at 25°C(a and b) and 20°C (c and d). Bar size is 100 μm for (a) and (b), 50 μm for (c) and 10 μm for (d). Holes and polygonal network structures are seen in both the cases.

3.9 Features observed in the central region when a 0.7mm thick solvent layer placed over a 230nm film is allowed to evaporate in ambient at 25°C (a) and 20°C (b,c, d, and e). Bar size is 10 μm for all images. At 20°C all different stages of dewetting is seen. While only holes (a) are seen at higher temperature (25°C), polygonal network structures (d) and droplets (e) are seen at 20°C.

3.10 Comparison of the feature observed when a 0.7mm thick solvent layer placed over a 50nm (a), 115nm (b), and 230nm (c) thick polystyrene film is allowed to evaporate in ambient at 25°C (i) and 20°C (ii). Bar size are 30 μm, 50μm and 10μm for (a), (b) and (c) respectively.

3.11 Rupture of a solvent film placed over a 50nm polystyrene film at 20°C. The initial solvent layer was 0.7mm thick and it took 12minutes to rupture. The optical micrographs are taken (a) 0.0 sec. (b) 0.56 sec. (c) 0.96 (d) 1.68 (e) 2.24 and (f) 3.12 sec after the rupture of the film.

3.12 Rupture of a solvent film placed over a 115nm polystyrene film at 25°C. The initial solvent layer was 0.7mm thick and it took 5 minutes to rupture. The optical micrographs are taken (a) 0.0 sec. (b) 2.0 sec. (c) 4.0 (d) 6.0 (e) 8.0 and (f) 10.0 (g) 12.0 sec and (h) 14.0 sec after the rupture of the film.

3.13 Optical Micrographs of the rims obtained due to stick slip motion of the retracting liquid layer over a 50nm (a), 115nm (b) and 230nm (c) thick polystyrene film at 25°C. Bar size are 50 μm for a(i) and b(i), 30 μm for a(ii) and b(ii), 100 μm for c.

3.14 Optical micrographs of the rims obtained due to stick slip motion of the retracting liquid layer over a 50nm polystyrene film at (a) 25°C and (b) 20°C. Bar size is 50 μm. Parallel lines of polymer droplets are seen at both the cases.

3.15 Optical Micrographs of the rims obtained due to stick slip motion of the retracting liquid layer over a 50nm polystyrene film at 25°C. The images are at a distance 4.5mm (a), 7.9mm (b), and 9.4mm (c) from the centre. Bar size is 50 μm. The polymer rims are seen to disintegrate into polymer droplets.

3.16 Optical micrographs of the parallel array of polymer dots produced during retraction of the solvent layer. Pattern (a) and (b) are observed in the central region, while (c) and (d) are observed in the region between two rims for a 115nm film at 25°C and 20°C respectively. Pattern (e) is observed for a 50nm film at 25°C.

3.17 Optical micrographs of the polymer ridges obtained during retraction of a solvent layer placed over a 30nm thick polystyrene film on silicon substrate at 20°C in presence of a 500 ml/m Nitrogen flow rate. On enlarging, (image b) polymer droplets are visible in between the ridges. Bar size are 100 μm and 10 μm for (a) and (b) respectively.

3.18 Optical micrographs of different features obtained, when a 1.0mm solvent layer placed over a 30nm polystyrene film on silicon substrate is allowed to evaporate in presence of a nitrogen flow of 500 ml/m. The images are at (a) 0.0mm (b) 1.0mm (c) 2.5mm (d) 3.0mm (e) 4.0 and (f) 4.5mm away towards the flow outlet from the centre. At the centre no features were observed. As we go towards the

periphery polymer drops, Polygonal cellular structures and finally holes were observed. Bar size is 10 μm.

3.19 Rupture of a solvent film placed over a 30nm polystyrene film on silicon substrate at 20°C. The initial solvent layer was 1.0mm thick and it took 8 min and 40 sec minutes to rupture. The optical micrographs are taken (a) 0.0 sec. (b) 6.0 sec. (c) 8.0 (d) 10.0 (e) 11.0 and (f) 12.0 (g) 13.0 sec (h) 15.0 sec after the rupture of the film. Image size is 937 μm x 705 μm. Interference fringes are due to thickness variation.

3.20 Optical micrographs of the features obtained when a 1.0mm solvent layer placed over a 30nm polystyrene film on silicon substrate is allowed to evaporate under a nitrogen flow of 200ml/m. Different features viz. (a) Polymer drops at the centre (b) polymer ridges away from the centre and (c) parallel array of polymer drops near the periphery are observed.

3.21 Optical micrographs of the features observed at the central region when a 0.7 mm solvent layer placed over a ~45nm polystyrene film on Quartz substrate is allowed to evaporate at 25°C (a and b) and 15°C (c and d) under different flow rate of nitrogen. Polymer droplets are seen for both the cases with 200ml/min (a) and 1050 ml/min (b) flow rate at 25°C. No features are observed with 0ml/min flow (c) and polygonal network disintegrating into droplets are seen with 500 ml/min flow (d) of nitrogen at 15°C. Bar size is 30 μm for a and b, while it is 50 μm for c and d.

3.22 Optical micrograph of a sequence of formation of parallel array of polymer droplets during retraction of the liquid layer or three phase contact line. Images are taken at 16 seconds interval. The size of the images is 937 μm x 705 μm.

4.1 Schematic of the arrangement where the polystyrene film is exposed in saturated solvent vapour within a dessicator. Solvent (toluene) is kept in a petridish at the bottom and polymer film is kept above it on a stand within a small petridish.

NOMENCLATURE

a : Activity

c_1 : Numerical constant, value 7.98

c_2 : Numerical constant, value 5.32

d_0 : Equilibrium distance between surfaces

h : Film thickness

n_f : Fraction of the original mass collected in the polygonal ring

v_S : Solvent molar volume

A : Hamaker constant

A_{eff} : Effective Hamaker constant

A_{ij} : Hamaker constant for molecules of type i and j

D_d : Diameter of the polymer drops

D_P : Diameter of the polygons

K : Bulk modulus of polymer

N_C : Average no of initial holes that combine to form a polygonal cell

N_D : No of polymer droplets per 10000 μm^2 area

N_H : Initial no of holes per 100000 μm^2 area

P_{VS} : Saturated vapour pressure of the solvent in equilibrium with solution

P_{VSO} : Saturated vapour pressure of the pure solvent

R : Universal gas constant

S^{LW} : LW componemt for the spreading coefficient for the substrate

T : Room temperature in Kelvin

T_g : Glass Transition temperature

$T_{G/PS}$: Glass Transition temperature of polymer/solvent

T_{G0} : Glass Transition temperature for dry polymer

T_{GS} : Glass Temperature of solvent

V_f : Free volume of polymer

Greek Letters:

γ : Surface Tension

λ_d : Dominant wave length

φ : Effective interface potential, excess free energy per unit area to bring two interfaces from infinity to a certain distance h.

φ_{vdW} : Non-retarded van der Waals potential

φ_{SR} : Short range interaction potential

Φ_P : Polymer volume fraction

Φ_{PG} : Polymer volume fraction at which glass transition take place

Φ_{SG} : Solvent volume fraction

CHAPTER 1

INTRODUCTION:

1.1 Definition of thin films:

A liquid film is formed when two interfaces of a liquid are in close proximity. In the surface between two macroscopic fluid phases, the intensive thermodynamic properties gradually change when passing from one phase to the other. In liquid film whose thickness is less than the effective range of intermolecular interactions, two surface region overlaps, thus affecting the properties of two surfaces. Usually films than 100nm have intensive thermodynamic properties that depend on thickness. These films are called THIN FILMS. In thin films the free energy arises out of contribution from excess intermolecular interactions and interfacial tensions, whereas free energy of relatively thicker film (>100nm) arise because of the interfacial tension only [1].

1.2: Application of thin films:

Thin films are abundant in life. Their importance and use in science and technology are increasing everyday. Thin films are important in lots of technological applications such as polymer and metal coatings, soft material nanostructures and play an important role in certain physical and biological phenomenon such as wetting, adhesion, heterogeneous nucleation, colloids, foams/emulsions/floatation, membrane-morphology, dry eye syndrome etc. Volatile and non-volatile thin films are present in many industrial processes such as floatation, polymeric and metal coating of surfaces, trickle bed reactor, contact equipment for heat and mass transfer [2-5]. Thin films find abundant use as coatings to tailor surface properties of substrate e.g. as photographic films, paints adhesives, dielectric, biocompatible and optical coatings and as microelectronic and optoelectronic devices [2-5]. Thin films also play important roles in stability of foams and emulsions [6-7]. The coalescence and lifetimes of foams and emulsions are controlled by the drainage and instability of thin liquid films in bubbles and drops. A variety of thin film phenomena are involved in the enhanced oil recovery [8] and thin film lubrication [9]. In the field of biomedical sciences and engineering, thin film stability and patterns are important in cell adhesion and engineered biomaterials [10-13]. Wetting of the cornea the thin tear film is a still an unresolved problem that is related to so-called dry eye syndromes. Thin mucus and aqueous coatings of the cornea can

become unstable in dry eyes, and the hydrophilic ingredients of dry eye solutions are engineered to restore the stability of the protective tear film [10, 11, 13].

1.4 Stability of thin films:

While macroscopic films are stable, the dewetting behaviour of mesoscopic thin films depends on whether the film is unstable or metastable [45]. On a theoretical basis, it is the sign of the curvature of the effective interface potential φ"(h) determining its stability. Containing short as well as long range interactions, it is defined as the excess free energy density which is necessary to move two interfaces from infinity to a certain distance h. This distance between the solid–polymer and polymer–vapour interfaces is a measure for the film thickness and is generally the order parameter of the system. A film is unstable if φ"(h) is negative. Otherwise it is metastable or stable.

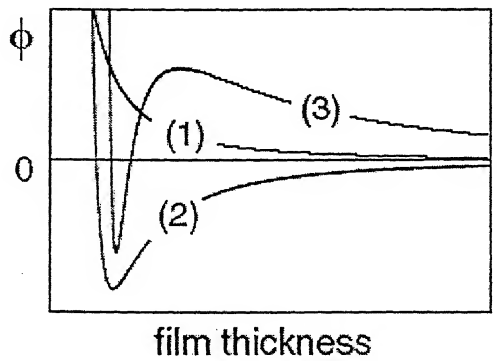

FIG. 1. Sketch of the effective interface potential $\phi(h)$ as a function of film thickness for stable (1), unstable (2), and metastable (3) films.

In the metastable case the system has to overcome a potential barrier in order to reach its state of lowest energy. The film ruptures due to a nucleation process. Far away from the sign reversal of φ"(h) it requires the presence of nucleation sites (heterogeneous nucleation) or otherwise a thermal activation can be sufficient to overcome the energy barrier (homogeneous nucleation). In contrast, an unstable film ruptures spontaneously via a spinodal mechanism. A small fluctuation in the system order parameter gives rise to instability. In a mean field approach with simplification to linear calculations, thermally activated capillary waves at the polymeric surface grow exponentially [14]. In analogy to the spinodal decomposition of a binary blend, the fastest growth mode destroys the film, giving

rise to one dominant characteristic wavevector. Anyway, the accuracy of the prediction of the boundary between unstable and metastable states depends on whether the correct form of the effective interface potential $\varphi(h)$ is known. In addition, within a linearly unstable range, instability-dominated and nucleation-dominated subranges have to be distinguished [15,16].

For apolar polymers on substrates, the most widely used long range part of the interaction is the non-retarded van der Waals interface potential

$$\varphi_{vdW}(h) = \frac{A_{eff}(h)}{12\pi h^2} \qquad \text{.....1.1}$$

The effective Hamaker constant $A_{eff}(h)$ replaces the common Hamaker constant 'A' which describes a simple two body interaction. For a liquid 'L' on top of a semi-infinite wall 'W', from the approximation $A_{ij} = A_{ii}\, A_{jj}$ the effective Hamaker constant $A_{eff}(h) = A_{LW} - A_{LL}$ is calculated to be independent of the film thickness, whereas this dependence shows up from the addition of a top layer O with thickness d covering the substrate:

$$A_{eff}(h) = A_{OL} - A_{LL} - \frac{(A_{OL} - A_{SL})}{(1 + d/h)^2} \qquad \text{.....1.2}$$

It accounts for a more complex substrate structure as introduced by coating layers [17]. A positive Hamaker constant repels the interface and favours a thick wetting layer of the polymer film. Recent work focused on the short ranged contributions in addition [18,19]. The distortion of the density profile in the vicinity of the substrate gives rise to this part of the effective interface potential. According to the work of Müller *et al* [18], it decays exponentially as the distance between the interface and the substrate grows. The order of the decay length is set by the characteristic length scale ξ of the interface profile and the magnitude of its strength is set by the tension γ of the interface between the polymer liquid and its vapour:

$$\frac{\varphi_{SR}(h)}{\gamma} = a \exp(-h/\gamma) - b \exp(-2h/\gamma) + \exp(-3h/\gamma) \qquad \text{.....1.3}$$

where, a and b are coefficients of order unity. Short ranged forces dominate on length scales

smaller than about $h \sim \xi \ln(\gamma / \varphi(h))$. Alternatively, other model potentials of the long and short ranged contributions were chosen [19]. In summary, the interplay between short and long ranged forces can yield a quite complex shape of the effective interface potential with several local minima [18].

1.4 Dewetting of thin films

The applications stated before often require a stable, homogeneous, uniform and durable film. Stability and morphological features of thin films on solid surfaces depend on the nature of short range and long range interactions between the film material and the solid substrate. Depending upon these interactions a film can be stable, unstable or metastable. Stability of thin films was widely studied. Unstable or metastable films relax towards a thermo-dynamical equilibrium yielding a rupture of the initially homogeneous film and holes results. These holes grow in lateral size, building a characteristic pattern, which decays further until a stable structure is reached. Frequently it is an assembly of the drops of film material, which replaces the initial film in the final state. This process is popularly known as DEWETTING.

1.5 Overview of the present work:

Dewetting, in most of the cases is an unwanted process in which a homogeneous thin film is destroyed. However if properly understood and controlled, it can be used for the fabrication of ordered patterns in micrometer and even in nanometer scale, which is otherwise a very difficult task for ordinary lithographic techniques. A large no of study has been performed theoretically and experimentally to explore the possibilities of forming ordered patterned using this easy to perform but complex process. Mostly polymeric films were used and whole lot of different configuration using various film material, different substrates, polymer blend films, bilayer films under different external conditions have been studied.

Although dewetting will occur for any liquid on a non wettable surface, films made of amorphous polymers are widely used for experiments due to the following reasons:

1. The high viscosity of the polymer allows time resolved experiments.
2. The vapour pressure is practically zero, thus ensuring minimum mass loss.
3. Thin and smooth films can be initially prepared and stored below glass transition temperature.

4. Polymer films enable a tailored viscosity to be obtained by variation of chain length and temperature.

In most of the recent studies dewetting of polymer film is induced by heating i.e by increasing the temperature above Glass Transition temperature. We tried dewetting of thin polymer film induced by solvent. Solvent was introduced in two different ways. Firstly as a liquid film over the thin polymer film and secondly the film is exposed in solvent vapour. Dewetting occurs in both the cases.

For the first case, a thin solvent (toluene) film ~1 mm was placed over the polymer (polystyrene) film with the help of a barrier and was allowed to evaporate. At the same time polymer gets dissolved into the solvent layer. With time the solvent film (having dissolved polymer in it) became thinner and thinner and finally ruptures. Depending upon the rate of evaporation and rate of dissolution different structures were observed. The structure formed due to rupture of film and during retraction of the three phase contact line freezes as the residual solvent evaporates leaving behind the dissolved polymer in it. This enables us to investigate the structures at later times. We studied the effect of polymer film thickness, temperature, Nitrogen flow rate on the various pattern formed. Parallel array of polymer dots can be produced by this method. An attempt has been made to find the dependency of the size of the polymer drops, spacing and distance between two parallel lines on the physical and environmental parameter of the system. Chapter 3 deals with it in details.

When thin polymer film is exposed in to solvent atmosphere at room temperature (25°C) [which is well below its glass transition temperature] the film dewets through formation of holes, hole growth, hole coalescence to form polygonal network structure which finally disintegrate into polymer droplets. A possible reason is proposed and the characteristic features are compared with the present theory of temperature induced dewetting. Chapter 4 deals with it in details.

Chapter 2 gives us a brief description of the tools we use to perform our experiments.

CHAPTER 2

TOOLS:

2.1 Sample preparation:

2.1.1 Material used: We used atactic Polystyrene (PS), obtained from Sigma-Aldrich Chemicals pvt. Ltd., New Delhi, as film material since it shows no crystallization, is chemically inert and has a low vapour pressure in the melt. As solvent HPLC grade toluene purchased from Spectrochem, Mumbai, India was used. Millipore-Milli-Q system, that uses Reverse Osmosis, EDI and filtration, provided the deionized (DI) water for cleaning. Reagent grade chemicals used during the substrate preparation, viz. 30% hydrogen peroxide, 27% ammonium hydroxide, trichloroethylene, acetone, methanol, hydrochloric, nitric and sulphuric acids were obtained from Qualigens Fine Chemicals and S.D. Fine-Chem Ltd., Mumbai, India and used as received.

2.1.2 Substrate preparation:

Three types of substrates were used for the experiments:

1. Glass slides from Blue star, Mumbai (7.5cm x 2.5cm x 1.3mm).
2. Quartz substrate obtained from Applied optics Inc., Bangalore (2cm x 2cm x 1mm both side polished)
3. Silicon wafer from Wafer World, USA with a native oxide layer as obtained from wafer world.

The substrates used for preparing films were cut into pieces with a diamond cutter in required size and kept in a slide holder (designed and made in-house). Then these substrates were cleaned thoroughly in the following procedure.

1. The slides (glass, Quartz or silicon) were dipped in detergent (laboline) solution for ten minutes and then both sides of the slides were thoroughly rubbed with a brush to

remove loose dirt on in. Then these are washed with DI water. The slides shouldn't be touched with hand this time onwards.

2. Then the slides, properly placed in holder were sonicated in detergent solution for 20 minutes. It was taken out and thoroughly washed with DI water for 3-4 times.
3. Then the slides were immersed in warm trichloroethylene (TCE) for 5 minutes. This and the next two solvent cleaning steps were performed to remove any organic contamination.
4. The slides were taken out and immersed in acetone for 5 minutes. This removes the TCE residues and acts as further cleaning solvent.
5. Then slides were immersed in methanol solution for 5 minutes. This removes the acetone residue. Then the slides were thoroughly washed with DI water to remove any residual solvents.
6. Then the slides were immersed in "ammonia-peroxide" solution for 15 minutes. The ammonia peroxide solution (or H_2O:H_2O_2:NH_4OH :: 5:1:1) prepared in the following way.

   First a mixture of H_2O and NH_4OH was taken in 5:1 ratio and was heated at around 70°C in a pyrex beaker for 10 minutes. Then the beaker was removed from hot plate and same amount of H_2O_2 as NH_4OH was added. The solution bubbled vigorously after 1-2 minutes and was ready to use.

   This step removed the residual organic contamination left over from the solvent cleaning. After this the slides were thoroughly washed with DI water. Now these were ready for acid cleaning. Glass and Quartz substrates were undergone a different acid clean procedure than the Silicon slides.

7a. For Glass and Quartz:

i. The slides were immersed in 30% (volume %)HCl solution taken in a polypropelene beaker for 30 minutes. HCl cleaned the substrate by mildly etching the surface. Then the slides were thoroughly washed with DI water.

ii. The slides were then dipped in 30% (volume %) HNO_3 solution taken in a polypropelene beaker for 30 minutes. HNO_3 cleaned the substrate by leeching the ions from within the surface of the substrate. Then the slides were thoroughly washed with DI water.

iii. The slides were then dipped in Aqua Regia ($HCl:HNO_3$::3:1) solution taken in a polypropelene beaker for 30 minutes. HNO_3 cleaned the substrate by leaching the ions from within the surface of the substrate.

Then the slides were thoroughly washed several times with DI water. Finally the slides were dried with flow of N_2/air and were used for coating films.

7b. For silicon substrates:

i. The slides were immersed in Chromerge solution for 20 minutes, taken out and thoroughly washed with DI water.

ii. The slides were then dipped in 30% HCl solution for 30 minutes to remove any residual Chromerge solution. The slides were then thoroughly rinsed with DI water several times and stored temporarily under DI water. The slides were taken out and dried with flow of N_2/air immediately before coating. If necessary sometimes the dried substrates were stored under vacuum.

2.1.3 Spin coating:

Spin coating is a common technique to uniformly coat a substrate with thin polymer layer. An adequate amount of polymer solution is placed onto a flat substrate held in place by a vacuum chuck. Subsequently it is rotated at a set frequency (single for a fixed time or series of different frequency for different time). Centrifugal force spreads the liquid evenly across the surface to a planar profile. The volatile solvent evaporates leaving behind a polymer film. Films of thickness from nanometer to micrometer can be prepared by this process. The thickness l of the resulting film depends on the viscosity, the polymer concentration, and the spin frequency ($l \propto \sqrt{1/v}$). The dimensions of the substrate are considered to be large compared to film thickness so as to neglect peripheral effects. For good solvents (e.g. PS in toluene) with slow rate of evaporation the resulting films are of excellent quality with an rms roughness of fraction of a nanometer, which is actually found (by examination under AFM) in our case. Two spin processors, PRS 4000 and programmable one (Model WS-400A-6TFM/lite/HSP) from Laurell Technologies Corporation, USA were used for the preparation of the films.

PRS 4000 Model: WS-400A-6TFM/lite/HSP

Figure 2.1: Spin Processors used for making films.

The film thicknesses obtained on different substrate from various concentration of polystyrene in toluene at different speed are tabulated below.

1. For PRS 4000

Substrate/size	Concentration Weight %	Amount added(microl)	Speed indicator	Time (seconds)	Thickness (nanometer)
Silicon/1.5x1cm	0.5	50	70	50	15
	0.5	50	40	50	20
	1.0	50	70	50	30-35
	1.0	50	40	50	40-45
	3.0	50	70	50	150
Glass/2x2cm	1.0	150	40	50	40-45
	2.0	150	40	50	110-120
	3.0	150	40	50	220-230

Table 2.1: Polystyrene film thickness made from different concentration at different spin speed with PRS 4000 spin processor.

2. For WS-400A-6TFM/lite/HSP from Laurell Technologies:

Substrate/size	Concentration Weight %	Amount added(microl)	Speed rpm	Time (seconds)	Thickness (nanometer)
Silicon/1.5x1cm	0.3	35	6000	50	12
	0.5	35	6000	50	20
	0.5	35	1500	50	30
	1.0	35	4000	50	45
	1.0	35	2000	50	50

Table 2.2: Polystyrene film thickness made from different concentration at different spin speed with spin processor WS-400A-6TFM/lite/HSP

On quartz similar range of thickness as on silicon substrate was obtained.

2.2 Film thickness measurement, Nulling ellipsometry:

Ellipsometry is a method of using reflected light to determine properties of surfaces and materials. Ellipsometry measures the change in polarization state of light reflected from the surface of a sample. The measured values are expressed as Ψ and Δ. These are defined as

$$\tan\psi = \frac{|R_{pp}|}{|R_{ss}|}$$

$$\Delta = \delta_{pp} - \delta_{ss}$$

where, R_{pp} and R_{ss} are the amplitude ratios of the reflected and incident 'p' and 's' components respectively. Similarly, δ_{pp} and δ_{ss} are the phase shift between incident and reflected 'p' and 's' components respectively. These Δ and Ψ values are functions of film thickness and optical properties of the layer stack from which reflection take place. So knowing the optical properties film thickness can be measured and vice versa. Also these values are related to the ratio of Fresnel reflection coefficients, R_p and R_s for *p* and *s*-polarized light, respectively by the following equation.

$$\tan(\Psi)e^{i\Delta} = \frac{R_p}{R_s}$$

Because ellipsometry measures the ratio of two values, it can be highly accurate and very reproducible. From the above equation the ratio is seen to be a complex number, thus it contains "phase" information contained in Δ, which makes the measurement very sensitive. In the **Fig. 2.2**, a linearly polarized input beam is converted to an elliptically polarized reflected beam. For any angle of incidence greater than 0° and less than 90°, *p*-polarized light and *s*-polarized will be reflected differently.

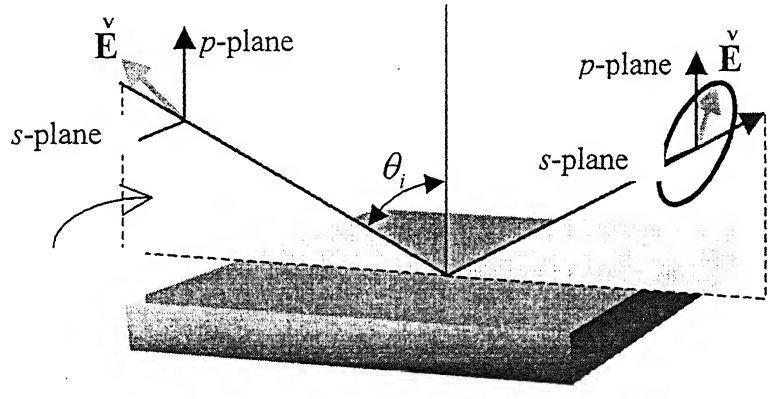

Figure 2.2: Schematic of the geometry of an ellipsometry experiment.

The coordinate system used to describe the ellipse of polarization is the *p*-*s* coordinate system. The *s*-direction is taken to be perpendicular to the direction of propagation and parallel to the sample surface. The *p*-direction is taken to be perpendicular to the direction of propagation and contained in the plane of incidence.

Null Ellipsometers use two polarizers: one on the source side of the sample (called the polarizer), and one on the reflected side, which is called the analyzer. The polarizer is followed by a retarder, which is usually a quarterwave plate. After going through the polarizer and retarder the light is in a known state of polarization. It then reflects from the sample surface, which changes its polarization. Since the analyzer is set to a certain polarization angle, only a portion of the reflected light will pass through to the photo-

multiplier tube detector. The polarizer and retarder can be adjusted to counter the change in polarization due to reflection off of the sample. These are adjusted such that the reflected light is linearly polarized (at a different angle than the analyzer setting). When this is adjusted properly there is no signal that reaches the detector. The whole arrangement is schematically shown below.

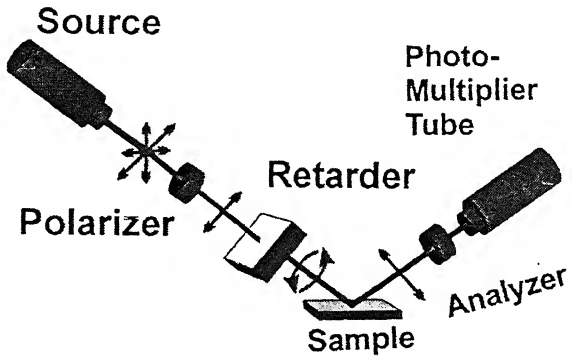

Figure 2.3: Schematic of a nulling ellipsometer

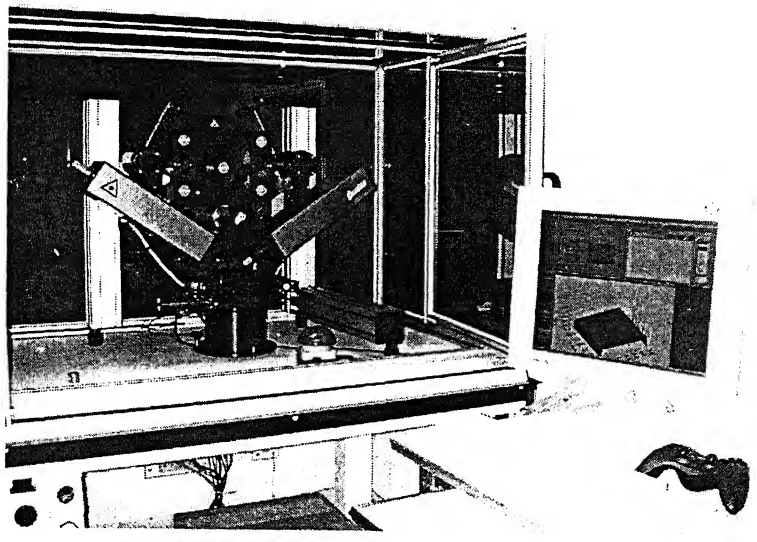

Figure 2.4: Front view of nulling ellipsometer from nanofilm, Germany

A typical measurement comprises of:

a) Setting the incident and reflected beam axes at some desired angle of incidence, referred henceforth as the goniometer angle θ, (generally about the Brewster angle θ_B of the system studied for maximum sensitivity) with respect to the sample aligned at the intersection of the two axes.

b) Obtaining the "null point" by rotating the polarizer followed by the rotation of the analyzer with the polarizer kept at the position of minimum intensity. The null point corresponds to a minimum in signal detected by the photo detector.

c) Determining at that "null" or "extinction" condition, the angular azimuths P of the polarizer and A of the analyzer with respect to the plane of incidence. The azimuths P and A at null are directly convertible by means of simple linear equations into the polarization parameters Δ and Ψ. The process can be repeated by varying θ about θ_B to obtain a set of values for Δ and Ψ.

d) Measured Δ and Ψ are however not useful as such as one is more interested in the various parameters of the film and/or substrate. So at this point one needs to range) to the formulae of Δ and Ψ expressed implicitly as a function of the film/substrate parameters and try to match (minimize MSE) the output Δ and Ψ of the model and the corresponding fit values (obtained from the measured (scattered) values of Δ and Ψ). Initially, this match is confirmed over a range of θ in the MAI (Multiple Angle Incidence) mode and the best fit values of the optical parameters are used subsequently in the SAI (Single Angle Incidence) mode.

Nulling Ellipsometer from nanofilm, Germany was used for measuring the film thickness and refractive index of the film.

2.3 Imaging

2.3.1 Optical microscope with CCD camera with computer interface:

An optical microscope (Model DMLM 100S) from LEICA Microsystem, Germany has been used for imaging both in situ and after experiment. Objects can be seen 50 to 1000 times magnified through it. It is equipped with both incident (for opaque objects) and transmitted (for transparent objects) light source. It has polarizer-IC prism arrangement which increases the vertical resolution so that the features become more prominent and visible without hampering its lateral magnification. Also there are different Filters viz.

ylight filter (DLF), grün, N16 which, in proper arrangement enhances the quality of the ıages. Images were captured by a CCD camera (Model no: SDC 4304PA) from Samsung erospace India Limited and a Digital Camera (Model: COOLPIX 990) from Nikon Japan. ifferent softwares viz. LEICA Qwin Standard Ver. 2.4, Nikon View 3.0, Adobe hotoshop Ver 5.0LE. MGI Vediowave Ver.1.51, Scion Image Ver. Beta 4.0.2 and ATI ideo player were used for capturing and analysis of the images.

.3.2 Atomic Force Microscopy:

ıtomic Force microscopy has evolved rapidly as an imaging tool for soft material with high patial resolution. The basic principle of the technique can be understood in the following vay: A cone or pyramid shaped tip usually made of silicon or silicon nitride (also cylindrical ısing carbon nano tube) is used as a probe. Upon approaching a surface the various interactions that can cause pressures in a thin film act now on the probe. Most importants are the van der Waals interactions (usually attractive), the steric repulsion, electrostatic Coulomb interaction, and capillary forces (attractive due to e.g. an absorbed layer of water or capillary condensation). As a result of the various interaction, the prove is exposed to an effective distance dependent force. The probe itself is attached to a cantilever with certain spring constant (typically 1-100N/m). By detecting the displacement of the cantilever the force acting on the tip can be measured.

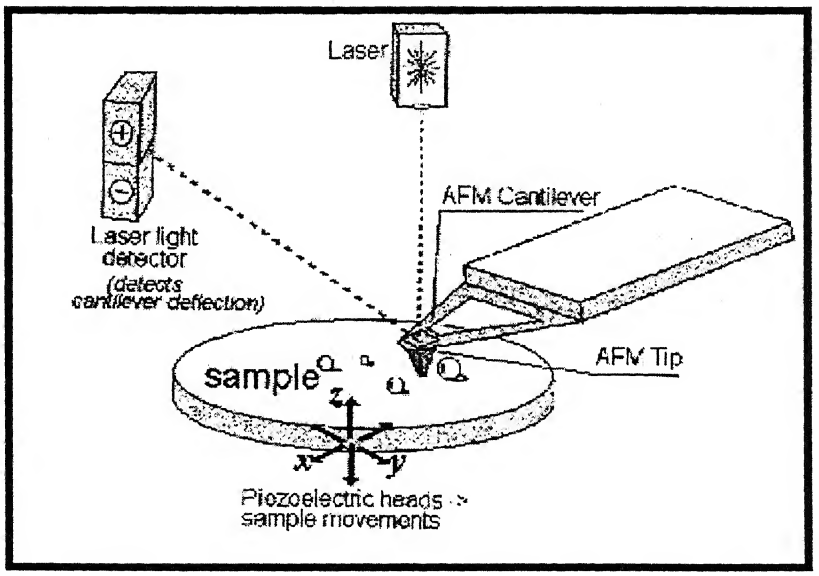

Figure 2.5: Schematic of Atomic Force Microscopy

A common technique to measure the cantilever displacement is the deflection of laser beam. A laser diode is focused on the back of the cantilever and the reflection is centered on a four Quadrant photo diode. The voltage difference of the upper and lower quadrants is proportional to the deflection. After calibration, absolute forces with the resolution of the order of 10^{-11} N can be measured this way. To image a sample, the tip is scanned relative to the sample. The feed back electronics keep the deflection of the beam constant by compensating change in topography by a piezo controlling the tip sample distance. The voltage applied to the piezo is then used to calculate the displacement of the piezo. The later is the mirror image of the sample topography.

2.4 Other Instruments:

i. Weighing Balance: Meter Toledo (AX105 Delta Range ®) electronic balance correct to five decimal places.

ii. Vibration Isolation Table: Vibraplane Model 9100/9200 series from Kinetic systems,

iii. Heating plate "HOTOP" from Tarsons.

iv. Vaccum Oven from Mahendra Instruments, Kanpur, U.P.

v. Goniometer from Rame-Hart Inc. NJ, USA for surface property measurement.

vi. Heating Stage with controller: Model TMH 94 from Linkam Scientific instruments Ltd.

vii. Refrigerator recirculator: Julabo F-30C, Germany

viii. Class 100 Clean bench: KlenzFlo®, Model 1500R, 48 x 30 x 30 from Klenzaids Bioclean Devices (P) Ltd., Mumbai.

ix. Fume Hood manufactured by Mahindra Instruments, Kanpur.

x. Vacuum pump: ILMVAC® diaphragm pumps, Germany.

CHAPTER 3

POLYMER PATTERNS IN EVAPORATING SOLVENT LAYER ON DISSOLVING SUBSTRATE.

3.1: Introduction:

Self organized polymer patterns obtained from a evaporating solution or suspension of particle is widely studied due to their potential to create nanometer-micrometer size ordered structure in a simple way. A large no of studies in this lines have been performed in recent years to investigate the potential of this process as soft lithography and also to understand the intricate mechanism behind this phenomenon in order to control them in a more productive way. A few observations are described below.

Sakurai *et al.* [20] observed undulation pattern similar to hexagonal cellular pattern produced by Rayleigh-Beńard convection in low viscous fluid on the free surface of a polymer film cast from solution, for poly (styrene-ran-butadiene) random copolymer and for mixtures of polystyrene and dioctylphthalate. They attributed this to the steady state convective flow in the polymer solution induced by solvent evaporation in earlier stage of casting and inhomogeneity of polymer concentration due to convection.

U. Thiele *et al.* [21] investigated the dewetting of an evaporating precursor (consists of collagen monomers in acetic acid) film on hydrophobic highly oriented pyrolytic graphite substrates. During drying the film ruptures and pores were formed which grows till all the solvent evaporates. Depending on the evaporation velocity of the solvent, different well-defined film morphologies have been observed. They attributed the two distinct peaks for pore radius distribution function to the occurrence of two distinct dewetting mechanisms: heterogeneous pore nucleation and spinodal dewetting.

S. G. Lipson *et al.*[22] presented a thermodynamic description of the dewetting process that can occur when a volatile film (water) evaporates from a substrate to which it is bound by both van der Waals and polar forces and showed that the initial stages of the pattern formation can be described in a manner analogous to the diffusion controlled solidification problem in two dimensions. For a range of values of vapour pressure a two phase system develops, involving the the coexistence of molecularly thin and macroscopically thick layers whose dynamics are controlled by vapour pressure. They used it to explain the origin of

experimentally observed spatial patterns in water films evaporating from clean mica substrates, where scale and other features are a function of the vapour pressure.
Few experiments were done with the polymer blend solution also.

Zdravko Mitov *et al.* [23] investigated the pattern formation and and droplet coarsening for ternary polymeric fluid in which phase separation was induced by solvent evaporation. For a particular range of solvent evaporation rates and thickness of liquid layers, ordered hexagonal patterns were formed at the liquid film-air interface. They ascribed this effect to Beńard-Marangoni convection induced by solvent evaporation and estimate conditions generating periodic two phase structures in polymeric films. They also observed that convection suppresses droplet coalescence and leads to a crossover in the coarsening rate of the monir phase from n= 0.89 to n= 0.67 in $R \sim t^n$.

Masato Yamamura *et al.* [24] investigated the ordered necklace like-like or cellular pattern formation from ternary polymer solutions in which primary and secondary phase separation was induced by solvent evaporation. The patterns consist of regular droplet arrays of various diameters, which arose in the pre-existing polymer phases via the secondary phase separation. The pattern formation is enhanced with increasing air velocity and ambient humidity, while it is suppressed with decreasing film thickness. The regular pattern is independent of surface wettability of the solid substrate. They ascribed the morphology change to the evaporation-induced surface tension driven convection, which rearrange the droplet distribution from disordered to flow-induced ordered patters.
A few studies were done with evaporating drops of polymer solution or suspension from a substrate. The famous "coffee-stain problem" studied by Deegan *et al.* [25,26] reported the formation of a ring deposit of particles by drying of a suspension drop formed due to the advection of the suspended particles towards pinned contact line. He also showed that when self induced pinning is the only source of pinning an array of patterns, including cellular and lamellar structures, sawtooth patterns arises from the dewetting and contact line pinning. Adachi *et al.* [27] reported the formation of concentric multiple rings of particles attributed to repeated pinning-depinning of the contact line.
Olaf Karthaus *et al.* [28] showed that ordered array of micron-sized polymer drops, sub-micron polymer dots or line structures on solid substrates can be produced from a evaporating drop of polymer solution. They attributed this to the stick-slip motion of the

receding contact line and Rayleigh instability of the fingers formed. Concentration difference near the three phase contact line is also believed to have an important role in it.
D. Raghavan *et al.* [29] reported the formation of Hele-Shaw patterns during dewetting of aquous, evaporating polymer{poly(acrylic acid)} solutions cast on glassy hydrophobic (polystyrene) substrates and commented that this type of dewetting-induced fingering instability generally observed when the dewetting rate and film viscosity are sufficiently large.

In all the previous studies, the self organized features have been studied with polymer solution or suspension on non dissolving substrate. The objective of this study is to study the self-organized patterns that result from the evaporation of an initially pure solvent layer on a dissolving substrate. A liquid solvent layer kept over a thin (<250nm) polymer film is allowed to evaporate in ambient and in controlled atmosphere. Depending upon the rate of evaporation and rate of dissolution of the polymer different patterns were observed after complete evaporation of the solvent. The structures formed due to rupture of the film freezes as the residual solvent evaporates leaving behind the polymer dissolved in it. This enables us to observe the patterns after completion of the process. The effect of polymer film thickness, temperature, Nitrogen flow rate on the pattern formed was investigated.

3.2: System of study:

A thin solvent (toluene) layer film was placed on a thin polystyrene film (coated on glass, Quartz or silicon substrate) and the solvent is allowed to evaporate. Solvent layer was kept over the polymer film confined within a barrier. The barrier was made of Teflon which is inert to toluene. The amount of solvent added was such that it shouldn't dry up too quickly to observe, also it wouldn't take too much of time so that all polymer dissolve in the solvent to form a homogeneous solution. Polymer dissolves into the solvent and simultaneously the solvent evaporates to make the solvent layer thinner and thinner. After sometime the liquid layer became so thin that it became unstable and ruptures. The rupture of the liquid film occurs at central region (having the thinnest liquid film) first due to the concave nature of the liquid film caused by capillary forces. The process is shown schematically in the figure below.

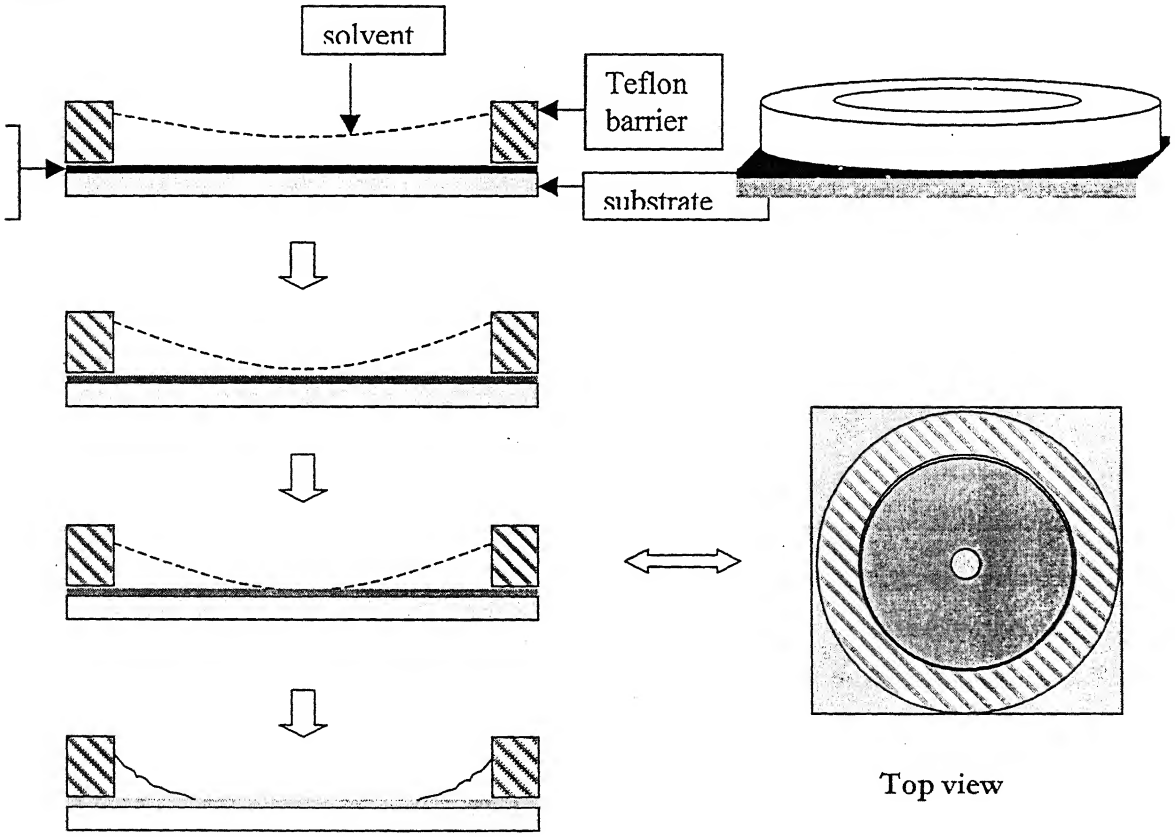

Figure 3.1: Schematic diagram of the process: The solvent film gradually thins up due to evaporation and ruptures from the centre

3.3: Experimental Section:

Polystyrene (MW 280000) was deposited by spin coating from toluene solution on glass, quartz or silicon substrate. By changing the concentration and spin speed we were able to prepare film of thickness 20-250nm [see Sec. 2.1.3]. Polystyrene was dissolved in toluene and heated a little to dissolve it quickly. Then the solution was filtered through a 0.22 μm filter to remove any dust particle. Then this solution was used for coating films. The substrates (Glass, Quartz and Silicon) were thoroughly cleaned in the procedure described in the sec. 2.1.2. Coating was done within a class 100 clean bench. After coating the films were stored under vacuum for 24 hours to remove and residual solvent. Then the films were annealed at 60°C for 6 hours to remove any strain that might have developed during the non-equilibrium spin coating process. The annealed film were quenched at room temperature (25°C) and stored under vacuum. Now films were ready to be used in the experiment. Film thicknesses were measured by nulling ellipsometry.

To keep a solvent layer over the polymer film different ways, such as just adding enough solvent to cover the whole film with the solvent layer pinned at the edges, and confining the solvent within a square and circular Teflon barrier have been tried. For the first case solvent layer gets de-pinned from the edges after some time and starts retracting towards the centre producing patterns formed due to contact line motion and pinning de-pinning phenomenon. The process is non uniform and hard to control. Also we were not able to produce the uniform thinning of the solvent layer which is the major objective of our experiment. So we use the second method which enabled us to achieve that, at least at the central region from where the film rupture took place. To prevent leakage the Teflon barrier was clipped at all the sides with coated substrate. This arrangement was used mostly for the experiment done in ambient with glass substrate. Both the configuration is shown below.

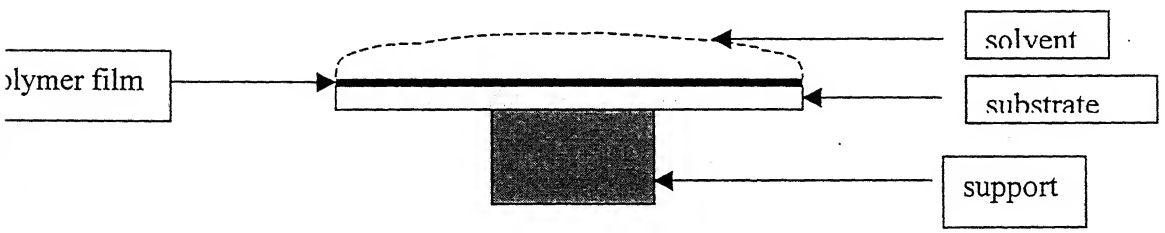

Figure 3.2: Solvent film placed over the polymer film pinned at the edges

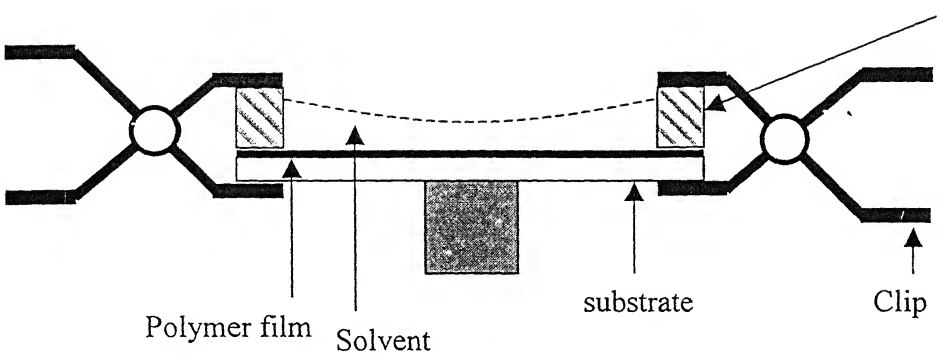

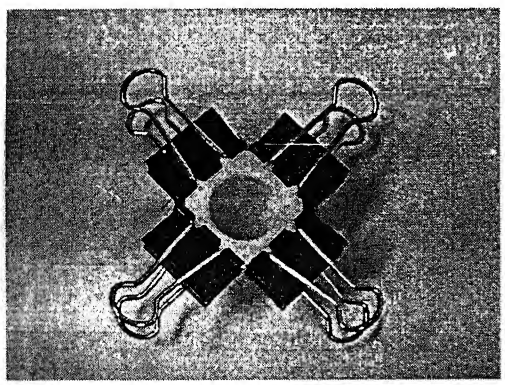

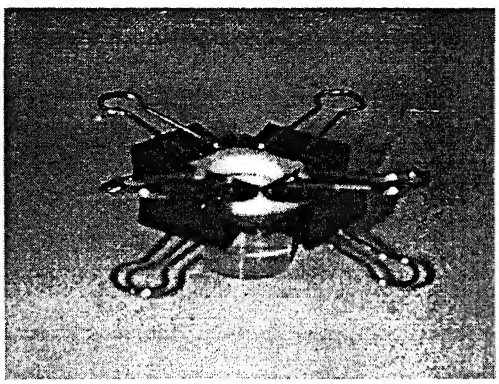

Figure 3.3: Schematic and digital image of the arrangement in which solvent film is confined over a polymer film within a Teflon barrier. The size of the substrate is 25mm x 25mm and inner diameter of the barrier is 19mm. Metal clips are used to prevent leakage.

Later we designed a chamber which serves the purpose of minimizing leakage, allow us to do experiments in confined atmosphere with various air/nitrogen flow rate and also make the simultaneous imaging of the process. The schematic and the actual setup are shown below.

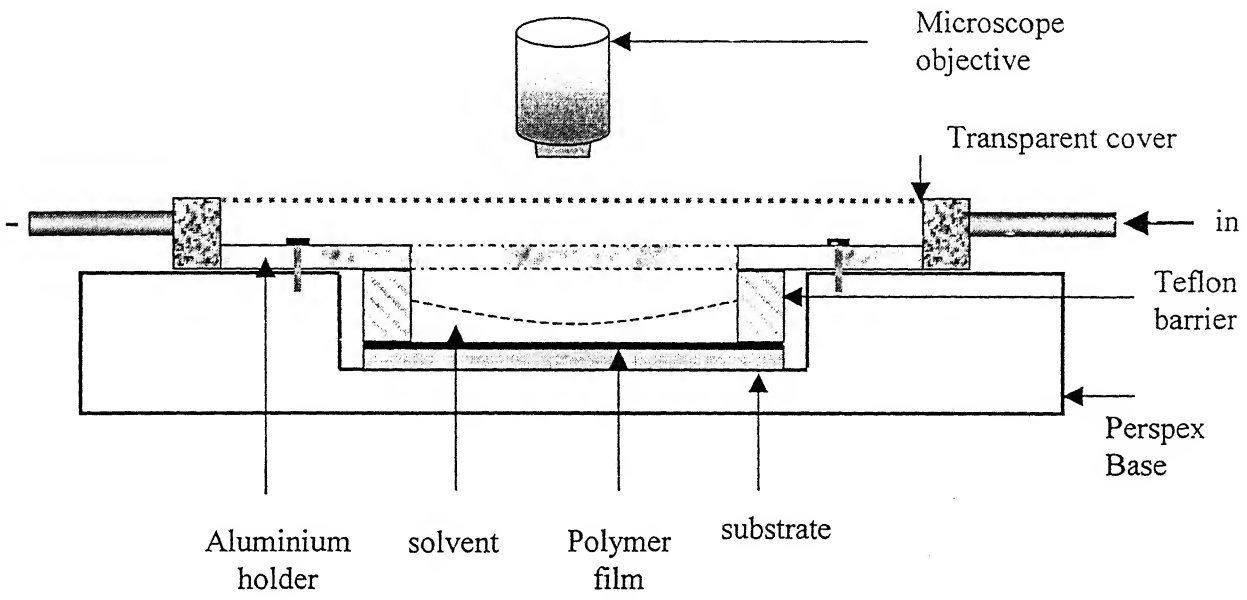

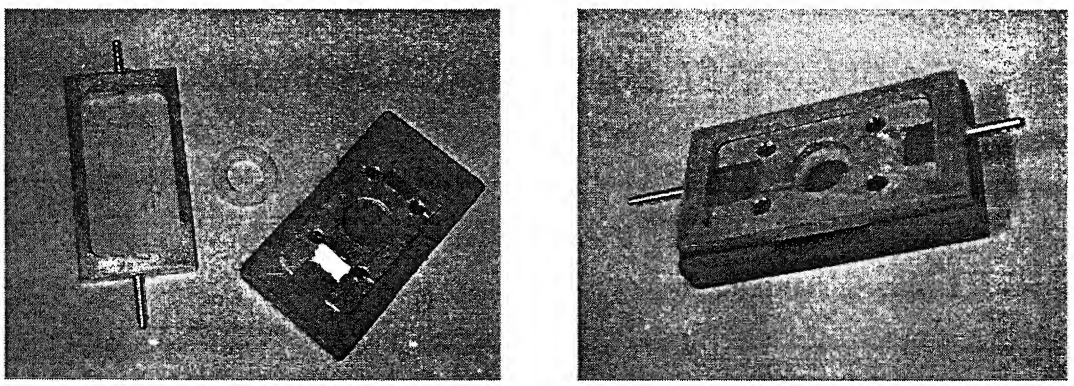

Figure 3.4: Schematic and actual experimental setup.

It consists of a base made of Perspex with a square groove to hold the coated substrate. The circular Teflon barrier was kept over the film and was held tightly by a square aluminum sheet (called holder) with the help of screws. The inner diameter of the barrier used was 19mm for glass and Quartz substrate and 15mm for silicon substrate. The holder has a

circular hole of equal size as the barrier. The whole system was covered by a transparent lid which exactly fits the holder to minimize air/nitrogen leakage. The lid has two openings at the far sides which act as the inlet and outlet for the air/nitrogen flow. Nitrogen flowrate was measured by a rotameter with a capacity from 100ml/min to 2000ml/min. We first fixed the barrier onto the film with the help of holder and screws. Then required amount of solvent was added and covered immediately with the transparent lid. The process was observed under microscope.

3.4 Results and Discussion:

A thin solvent (toluene) layer (~1mm) confined within a boundary was placed over a thin (30-250nm) polystyrene film. As toluene is a solvent for polystyrene it dissolves in it. Also having a moderate vapour pressure at operating temperature (20-25°C) there is loss of toluene due to evaporation. So the liquid layer (solvent along with dissolved polystyrene) gradually thins up. The rate of thinning depends upon the rate of evaporation of solvent which again depends on the rate of air flow rate, temperature, amount of dissolved polymer present etc. Gradually the liquid layer becomes so thin that it became unstable and ruptures to dewet the polymer film. The patterns formed from rupture of the film freezes due to evaporation of solvent, leaving behind the polystyrene dissolved in it. It helps to examine the structures at later stage. We had used a circular barrier so that the process is symmetric in all radial direction. Due to the concave nature of the surface of liquid layer the rupture took place near the centre of the barrier. This region is referred as "CENTRAL REGION". A circular liquid contact line form immediately after rupture and it retracts towards the boundary. The retraction speed gradually decreases away from the centre and after some time it stops retracting as the contact line is pinned at the substrate.

Three different substrates, glass, Quartz and Silicon were used for coating films. In each case different sets of experiments were performed to see the effect of different substrates. Experiments performed with each of the three substrates are described in the next three sections.

3.4.1 Evaporation of solvent (toluene) film placed over a thin (45-230nm) polystyrene film coated on glass substrate:

All the experiments were done in the arrangement shown in the figure 3.3 in ambient. A Teflon barrier of diameter 19mm was used. 200 microlitre toluene was added in all the cases which effectively make a ~0.7 mm liquid film over the polymer film. We have concentrated on the patterns formed during three distinct phase of the process. They are

1. Pattern formed during the rupture of the liquid film i.e in the so called CENTRAL REGIONS.
2. Pattern formed due to the stick-slip motion of the retracting liquid layer.
3. Pattern formed during continuous retraction of the liquid layer within the innermost ridge and also in between dominant ridges formed due to stick slip motion.

We have studied the effect of film thickness and temperature on the pattern formed during these three processes. The time for initial rupture of film was also noted down which gives us an idea for rate of evaporation.

4.1.1 Pattern formed at Central region:

3.4.1.1.1 Effect of film thickness on the pattern formed at central region:

For a particular temperature the pattern formed at the central region changes with film thickness. We compare the pattern formed at each experimental temperature for different thickness.

First at 25°C for lowest thickness film i.e 50nm thick film polymer droplets were observed while for both the higher thickness film, 115nm and 230nm holes were observed. The only difference between them is for relatively thinner 115nm film there are finger inside the holes while fingers are absent for 230nm film. Also the hole size is larger for 115nm (10-30μm) film than 230nm (1-6μm) film. The time for initial rupture of films gradually decreases with increasing film thickness which was 11min, 5min and 3.5min for 50nm, 115nm and 230nm films.

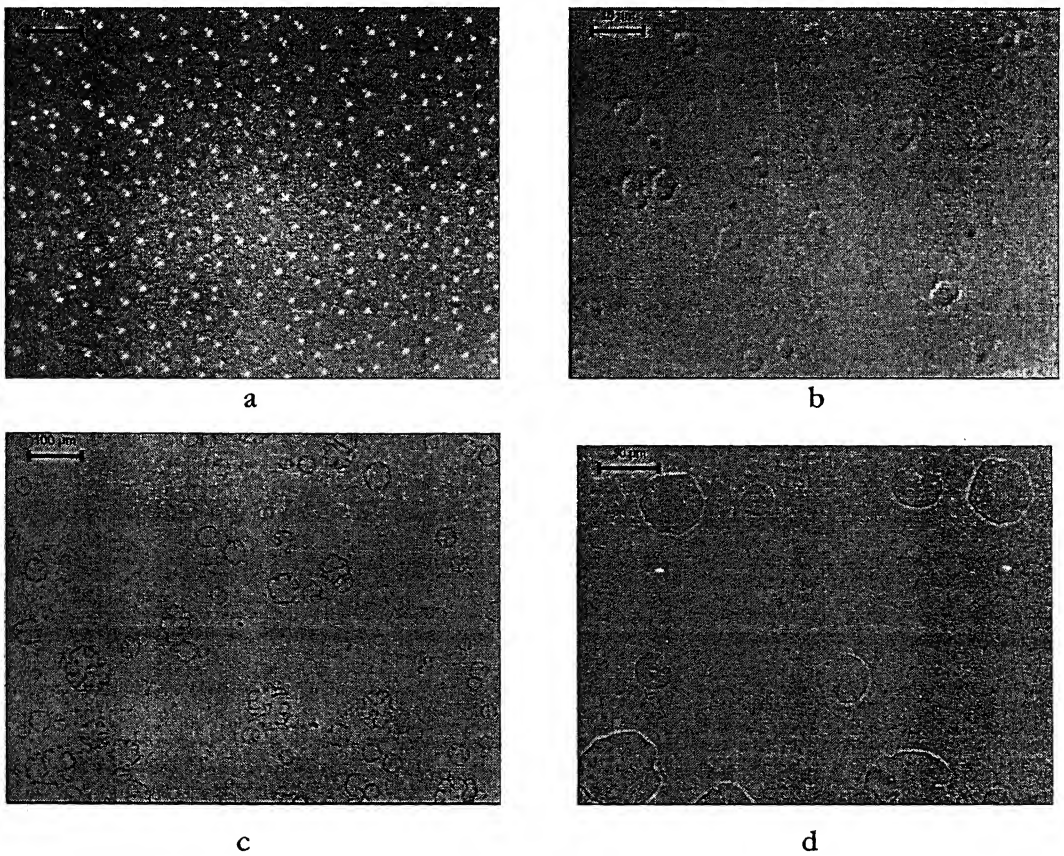

Figure 3.5: Features observed in the central region when a 0.7mm thick solvent layer placed over a. 50nm b. 230nm and c-d. 115nm thick polystyrene film was allowed to evaporate in ambient at 25°C. Bar size are 10 μm for (a) and (b), 100μm and 30μm for (c) and (d) respectively.

At 20°C the main difference is same as 25°C for different thickness. Only thing is that for higher thickness film the holes grows further to form polygonal ring structures and sometimes break up to form droplets. The time taken for rupture of film was 11 min, 9 min and 4.5 min respectively.

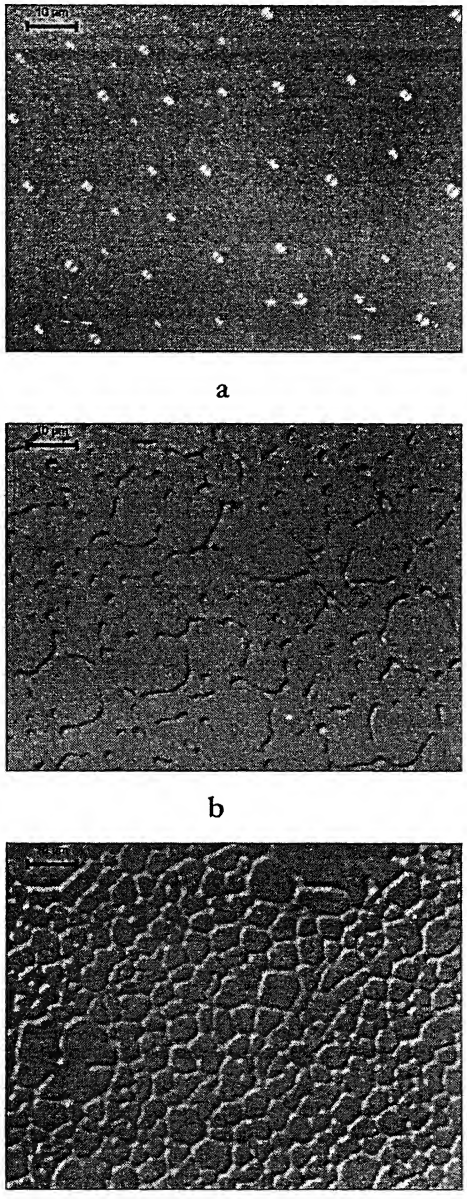

Figure 3.6: Features observed in the central region when a 0.7mm thick solvent layer placed over a. 50nm b. 115nm and c.230 nm thick polystyrene film was allowed to evaporate in ambient at 20°C. While for thinner film polymer droplets are seen (a) polygonal network structures are seen for thicker films (b and c). Bar size is 10 μm.

4.1.1.2 Effect of Temperature for a particular film thickness:

xperiments were done at two different temperatures 20°C and 25°C for each film ickness.

or 50nm thick films the main feature was found to be randomly oriented polymer droplets. he average no density of droplets was found higher for higher temperature, 53570/mm^2 nd 5600/mm^2 at 25°C and 20°C respectively. The average drop size was found smaller for igher temperature, 1.35 μm (varies from 0.5-2.1 μm) and 1.65 μm (varies from 0.88-2.70 m) at 25°C and 20°C respectively. The time taken for rupture of liquid film was pproximately 9 minute and 11 minute at 25°C and 20°C respectively. As the time

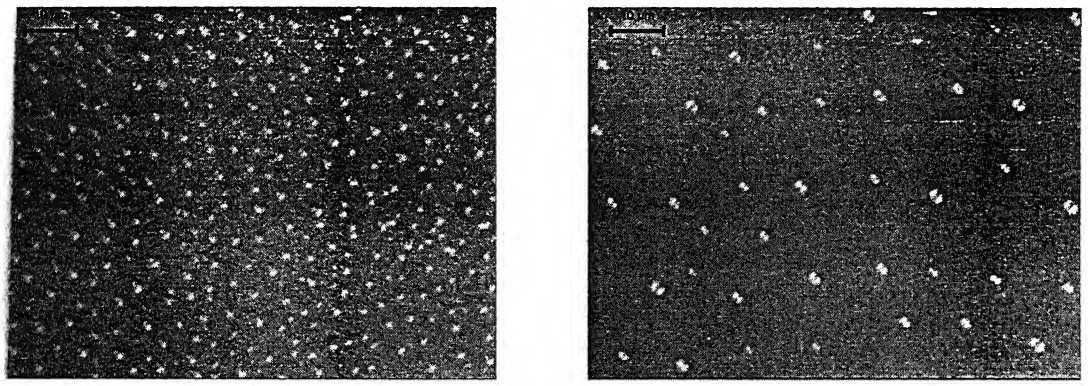

a. b

Figure 3.7: Polymer droplets observed in the central region when a 0.7mm thick solvent layer placed over a 50nm film is allowed to evaporate in ambient at a. 25°C and b. 20°C. No density of polymer droplets increases with increasing thickness. Bar size is 10 μm.

For 115nm films at 25°C holes with were seen at the point of rupture. Within the central zone away from the centre large holes coalesce with each other forming polymer droplets were seen. The holes have prominent fingers formed during retraction of the holes which sometimes breaks up into polymer drops due to Rayleigh instability. While at 20°C the main features were polymer droplets. The no density and average size were 42850/mm^2 and the last stage of dewetting i.e the polygonal rim structures broken into polymer droplets was also seen. The time for rupture of the liquid films at 25°C and 20°C were approximately 5 minutes and 9 minutes respectively.

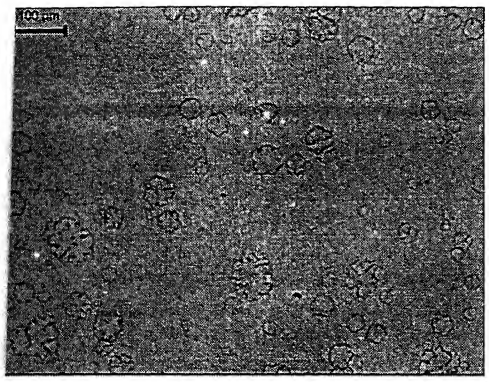

a

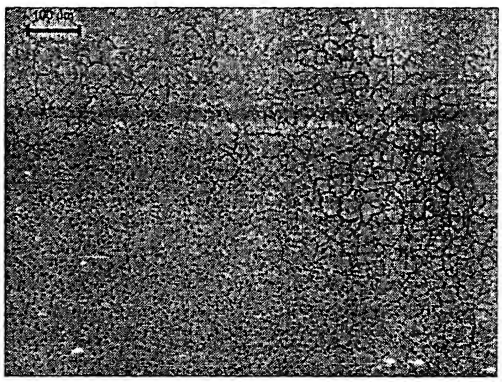

b

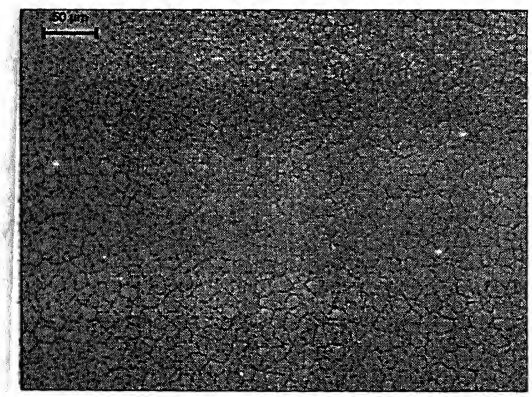

c

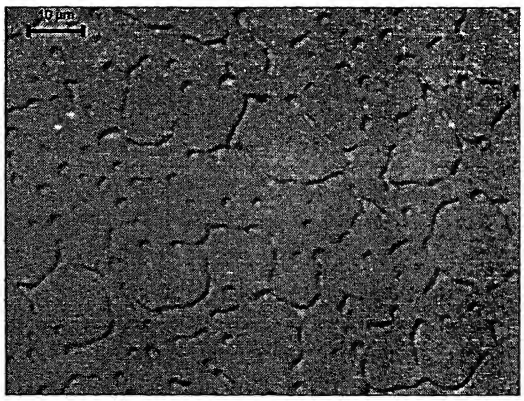

d

Figure 3.8: Features observed in the central region when a 0.7mm thick solvent layer placed over a 115nm film is allowed to evaporate in ambient at 25°C(a and b) and 20°C (c and d). Bar size is 100 μm for (a) and (b), 50 μm for (c) and 10 μm for (d). Holes and polygonal network structures are seen in both the cases.

or 230 nm film at 25°C a few holes from 1-6 μm size were observed. The average no ensity is found to be 4600/mm^2. At 20°C different stages of dewetting were observed ithin the central region. The average time for rupture of films at 25°C and 20°C were 3.5 inute and 4.5 minutes.

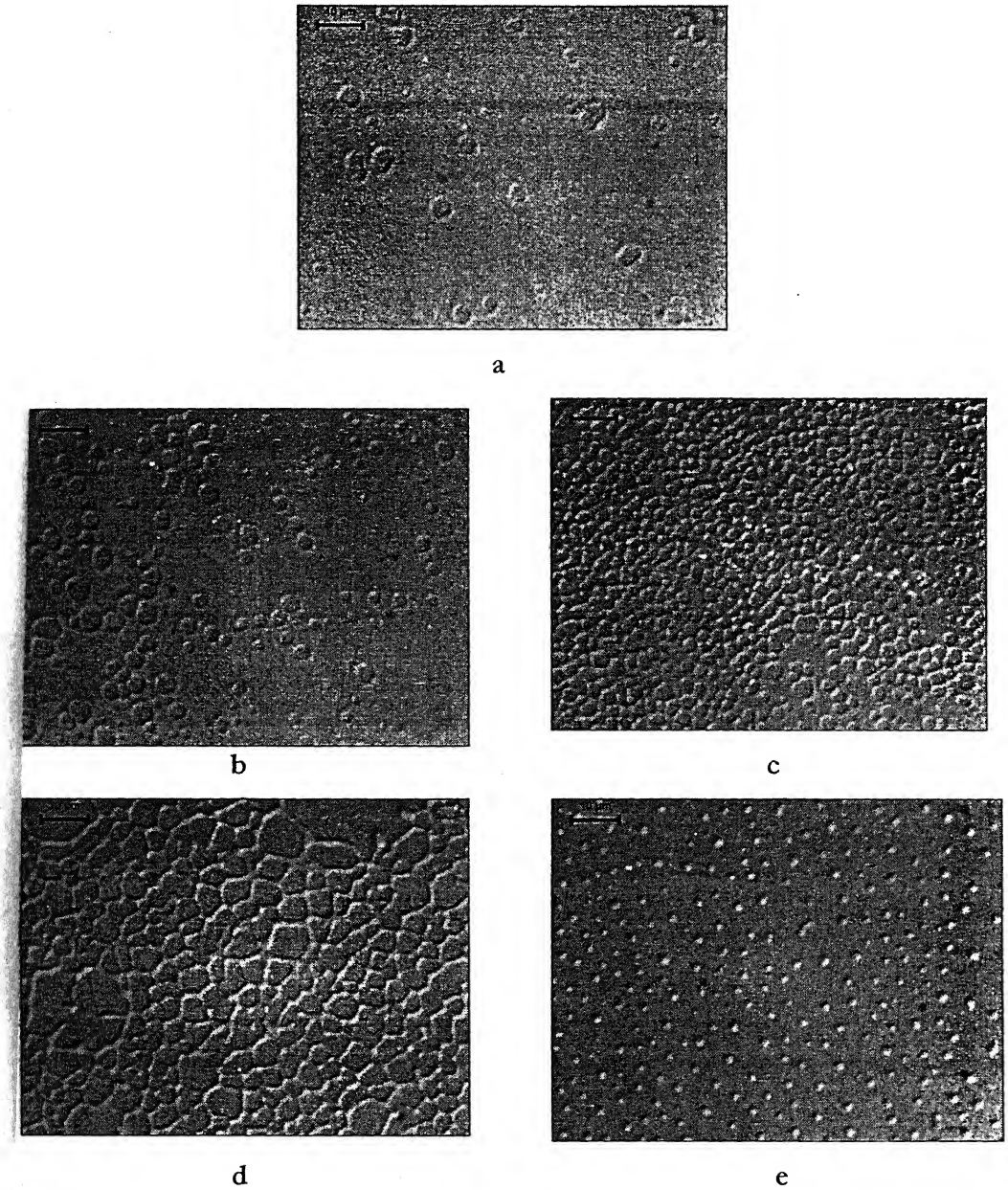

Figure 3.9: Features observed in the central region when a 0.7mm thick solvent layer placed over a 230nm film is allowed to evaporate in ambient at 25°C (a) and 20°C (b,c, d, and e). Bar size is 10 μm for all images. At 20°C all different stages of dewetting is seen. While only holes (a) are seen at higher temperature (25°C), polygonal network structures (d) and droplets (e) are seen at 20°C.

Comparison of patterns formed at central region for 50nm, 115nm and 230nm thick polystyrene film at 25°C and 20°C.

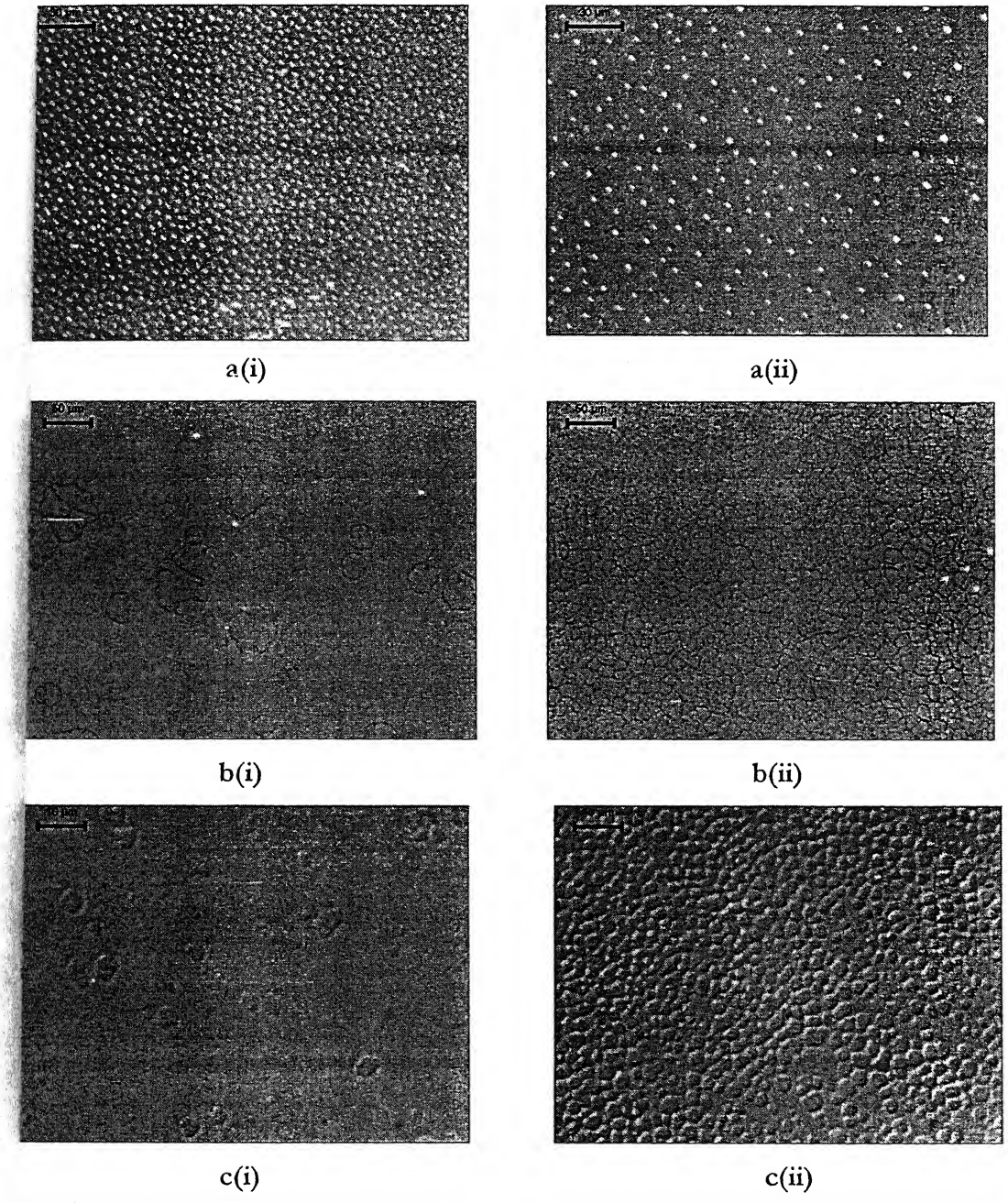

Figure 3.10: Comparison of the feature observed when a 0.7mm thick solvent layer placed over a 50nm (a), 115nm (b), and 230nm (c) thick polystyrene film is allowed to evaporate in ambient at 25°C (i) and 20°C (ii). Bar size are 30 μm, 50μm and 10μm for (a), (b) and (c) respectively.

1.1.3 Rupture sequence of the liquid layer placed over a 50nm film confined within a rier. The temperature was 20°C and time taken for initial rupture was 12minute.

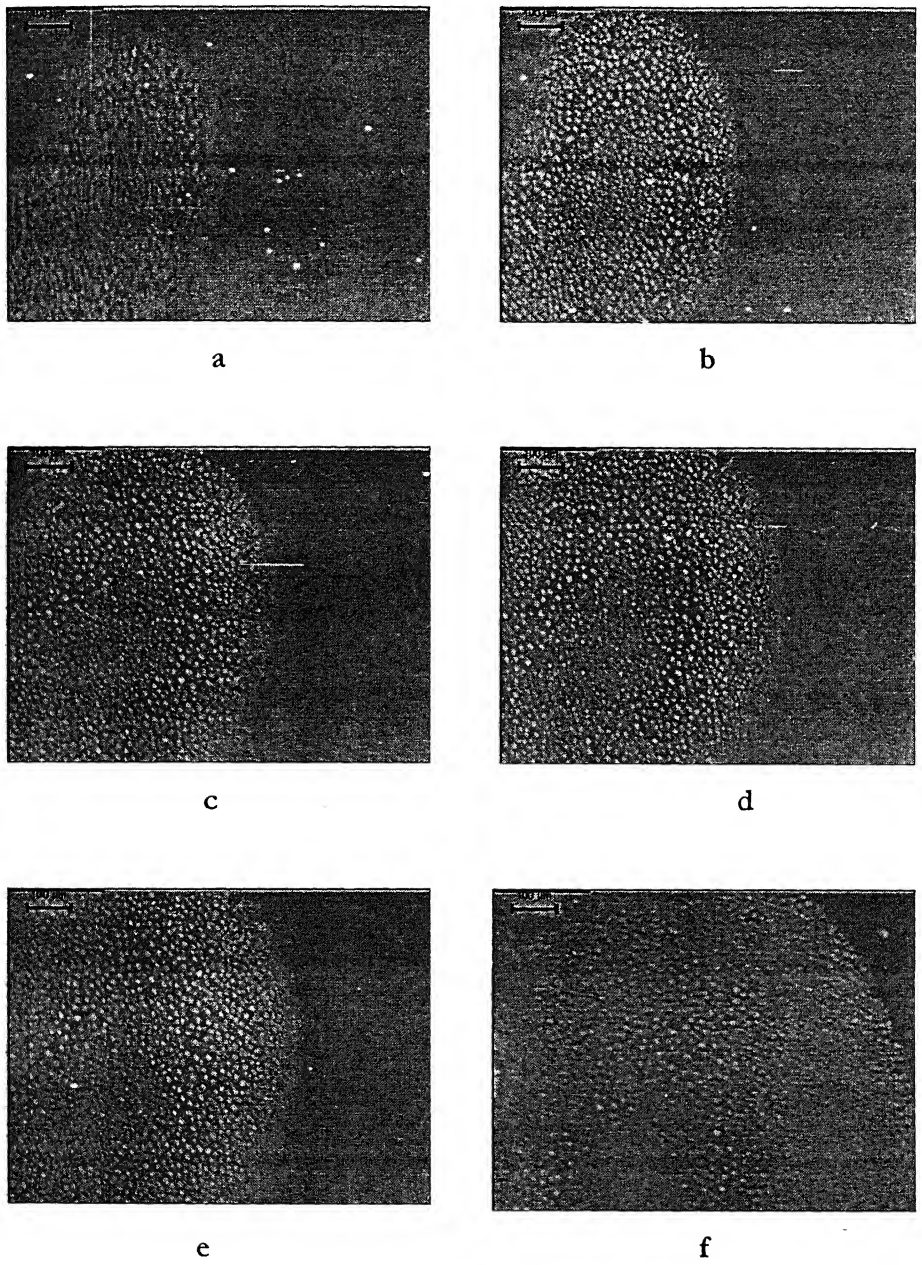

Figure 3.11: Rupture of a solvent film placed over a 50nm polystyrene film at 20°C. The initial solvent layer was 0.7mm thick and it took 12minutes to rupture. The optical micrographs are taken (a) 0.0 sec. (b) 0.56 sec. (c) 0.96 (d) 1.68 (e) 2.24 and (f) 3.12 sec after the rupture of the film.

upture sequence of the liquid layer placed over an 115nm film confined within a barrier. he temperature was 25°C and time taken for initial rupture was 5 minute.

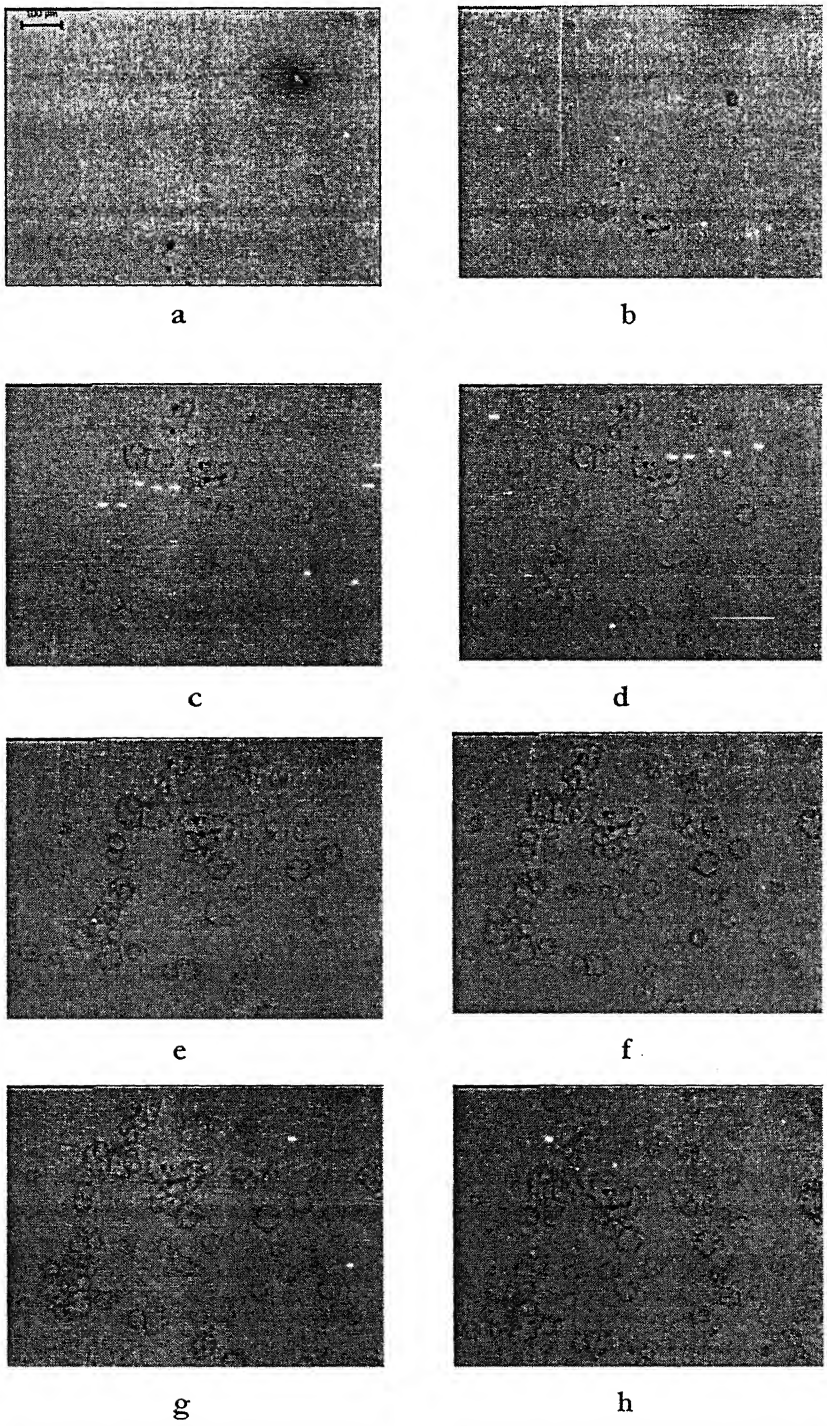

Figure 3.12: Rupture of a solvent film placed over a 115nm polystyrene film at 25°C. The initial solvent layer was 0.7mm thick and it took 5 minutes to rupture. The optical micrographs are taken (a) 0.0 sec. (b) 2.0 sec. (c) 4.0 (d) 6.0 (e) 8.0 and (f) 10.0 (g) 12.0 sec and (h) 14.0 sec after the rupture of the film.

.1.2 Pattern formed due to the stick-slip motion of the retracting contact line:

.1.2.1 Effect of film thickness on the rims formed:

r thinnest film i.e 50nm film the rims were not continuous and broken into fairly equally aced and circular polymer droplets. As we go towards higher thickness the rims become ntinuous undulated one as observed for 115nm film. For still higher thickness the rims ere thicker and of irregular shape.

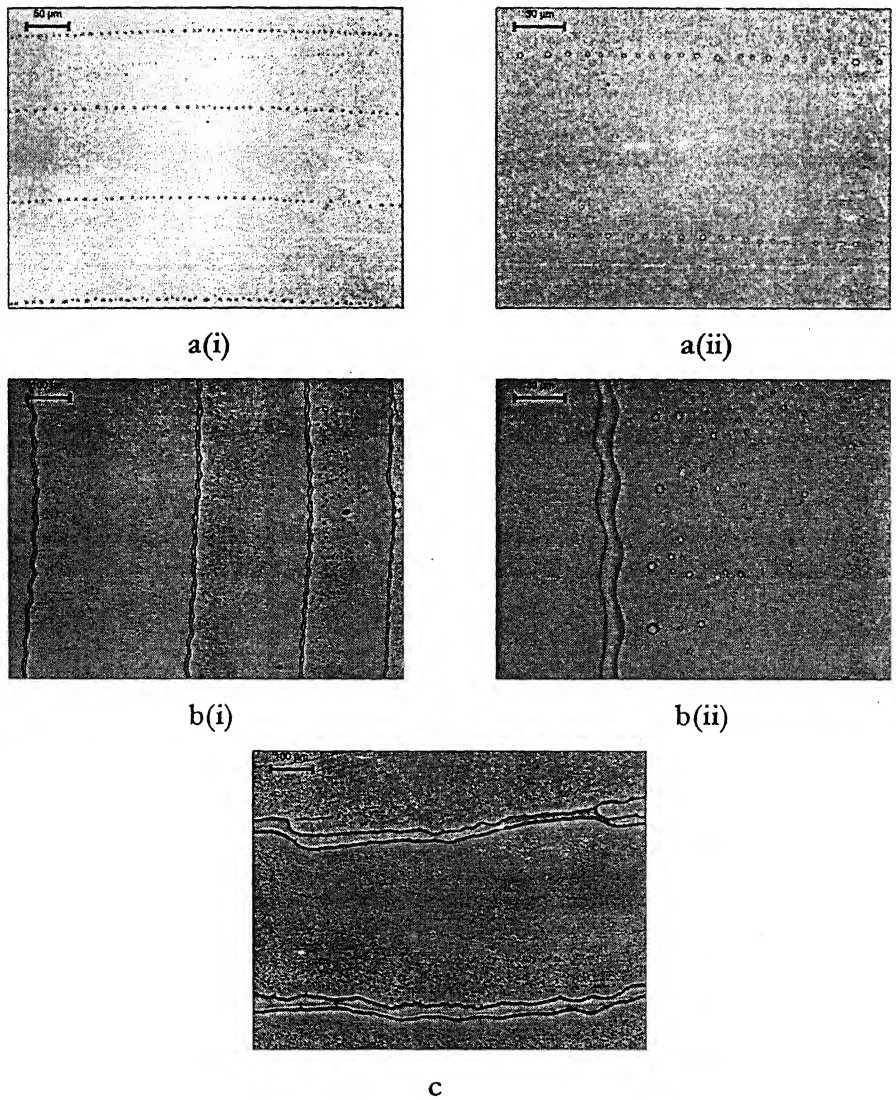

Figure 3.13: Optical Micrographs of the rims obtained due to stick slip motion of the retracting liquid layer over a 50nm (a), 115nm(b) and 230nm(c) thick polystyrene film at 25°C. Bar size are 50 μm for a(i) and b(i), 30 μm for a(ii) and b(ii), 100 μm for c.

.4.1.2.2 Effect of temperature:

t is observed that for a particular film thickness, if we decrease the temperature both the verage size of the polymer droplets formed due to breaking up of the rims and mean listance between them increases. As an example for a 50nm thick film at 25°C the average size and average distance between droplets are 3μm and 12.26μm respectively, while these values are 14.88μm and 46.34μm respectively at 20°C. The distance of rims is 8mm from centre for both cases.

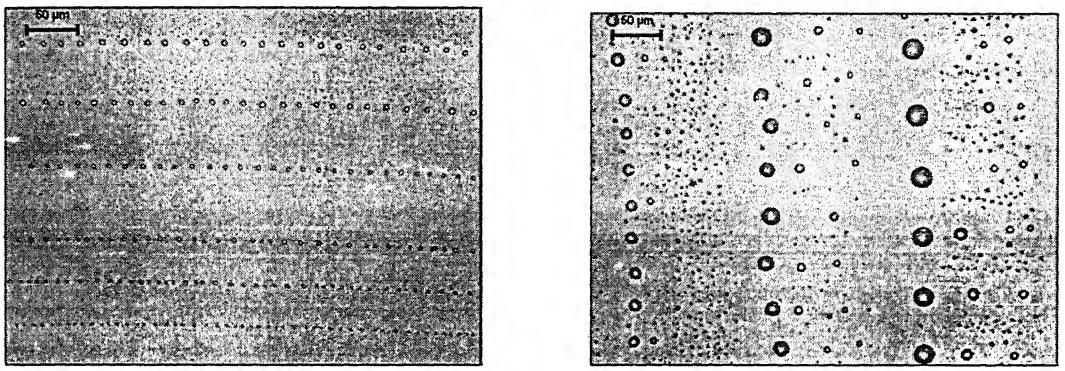

Figure 3.14: Optical micrographs of the rims obtained due to stick slip motion of the retracting liquid layer over a 50nm polystyrene film at (a) 25°C and (b) 20°C. Bar size is 50 μm. Parallel lines of polymer droplets are seen at both the cases.

3.4.1.2.3 Variation with distance from centre:

For a particular film thickness and temperature if we go towards the periphery both the size and mean distance between the polymer droplets increases. Also the average distance between two consecutive rims decreases. For a 50nm film at 25°C we observed the following:

Table 3.1: Variation of average dropsize, average distance between drops and average distance between consecutive lines for a 50nm film at 25°C.

Distance of the rim from centre (mm)	Average drop size (μm)	Average distance between drops (μm)	Average distance between consecutive rims (μm)
4.5	2.83	9.70	97.5
7.9	3.00	12.26	53.0
9.4	5.07	15.53	39.25

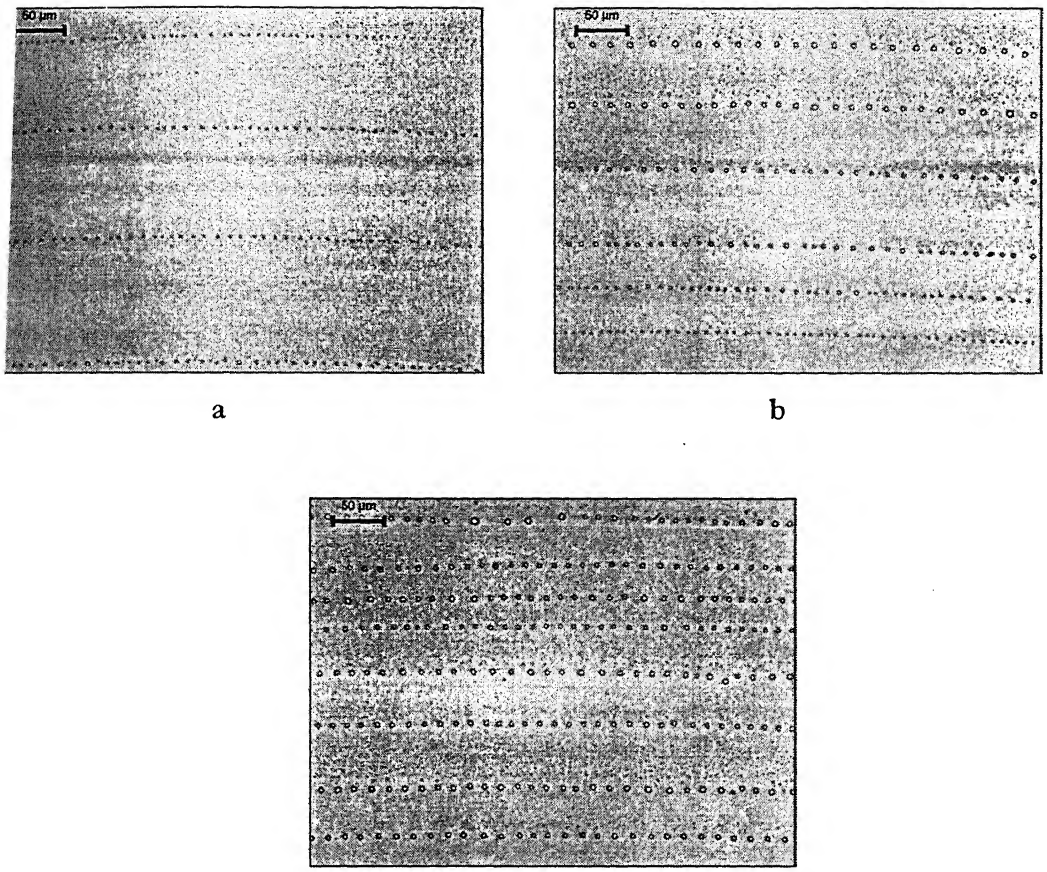

Figure 3.15: Optical Micrographs of the rims obtained due to stick slip motion of the retracting liquid layer over a 50nm polystyrene film at 25°C. The images are at a distance 4.5mm (a), 7.9mm (b), and 9.4mm (c) from the centre. Bar size is 50 µm. The polymer rims are seen to disintegrate into polymer droplets.

1.3 Pattern formed during continuous retraction of the contact line:

:he central zone and within two dominant ridges formed due to stick slip motion of the :acting line parallel array of polymer dots are observed. The polymer dots were of almost ıal size and placed equal distant from each other for a particular line. It is found that for a :ticular region as we go towards periphery the size and distance between the dots reases. Also the distance between two consecutive array increases as we go away from the ıtre. For 115nm these array of polymer dots were observed both in the central zone and thin ridges while for 50nm film no such patterns were found in region between two ridges. ıaracteristics of the different features observed for a 115nm polystyrene film are tabulated the table 3.1.

able 3.2: Average drop size, mean distance between the drops and average distance etween two parallel lines observed in the central region and region between two dges for an 115nm polystyrene film.

'emperature	Central region			In between ridges		
	Average Size of the drops (μm)	Average distance between drops (μm)	Average distance between two lines (μm)	Average Size of the drops (μm)	Average distance between drops (μm)	Average distance between two lines (μm)
25°C	2.5	10.7	19.08	1.8	6.93	11.07
20°C	1.0	3.5	5.08	1.24	3.45	5.3

The average drop size, mean distance between the drops and average distance between two parallel lines are 0.75 μm, 2.92 μm and 9.37 μm respectively for a 50nm polystyrene film.

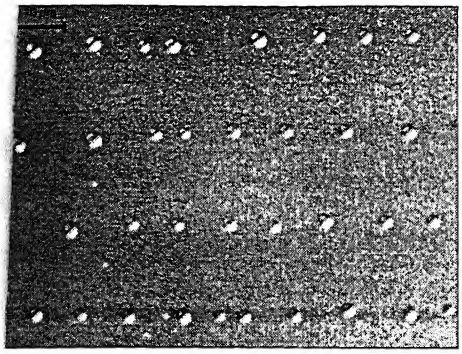

a

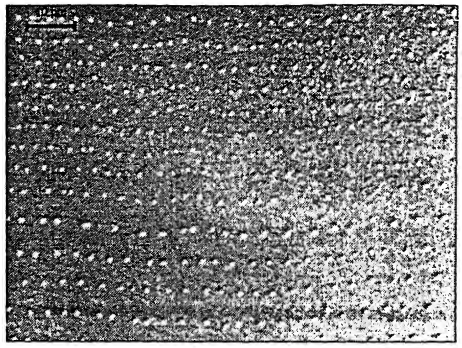

b

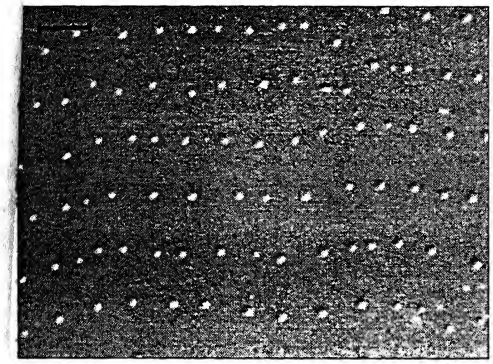

c

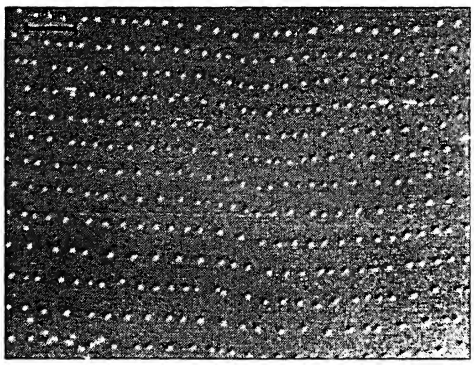

d

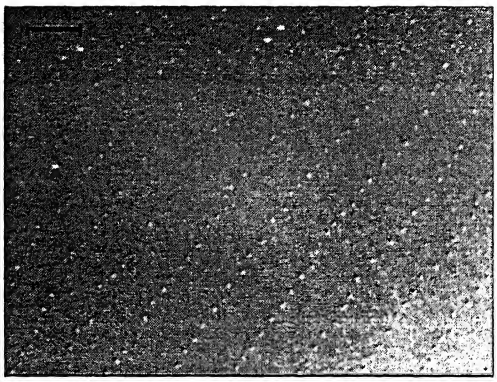

e

Figure 3.16: Optical micrographs of the parallel array of polymer dots produced during retraction of the solvent layer. Pattern (a) and (b) are observed in the central region, while (c) and (d) are observed in the region between two rims for a 115nm film at 25°C and 20°C respectively. Pattern (e) is observed for a 50nm film at 25°C.

3.4.2 Evaporation of solvent (toluene) film placed over a thin (35nm) polystyrene film coated on Silicon substrate:

All the experiments were done in the arrangement shown in the figure 3.4 in confined atmosphere with or without Nitrogen flow. Silicon wafers were cut into 2cm x 2cm pieces and a Teflon barrier of diameter 15mm was used. 175 microlitres toluene was added in all the cases which effectively make a ~1.0 mm liquid film over the polymer film. Here the experiments were done for approximately 32 (30-33nm) nm films at 20°C with different nitrogen flow rate. The main structures obtained for different Nitrogen flow rate is described below.

With a nitrogen flow rate of 500ml/min: The different features that were observed as we move gradually from centre towards periphery are shown in Figure 3.18. At the centre no features were observed. As we move towards the periphery first polymer drops, then polygonal cellular structure and then holes were found. The characteristics of different features are tabulated in the table given next. Although the arrangements of the features are same in all direction, due to flow of nitrogen the amount of polymer present towards the flow outlet is more than the inlet. It is obvious from the mean thickness of the region at same distance from centre as seen from the table. Polymer ridges seen near the periphery is shown in fig 3.17. The film ruptures after 8 minute 40 sec.

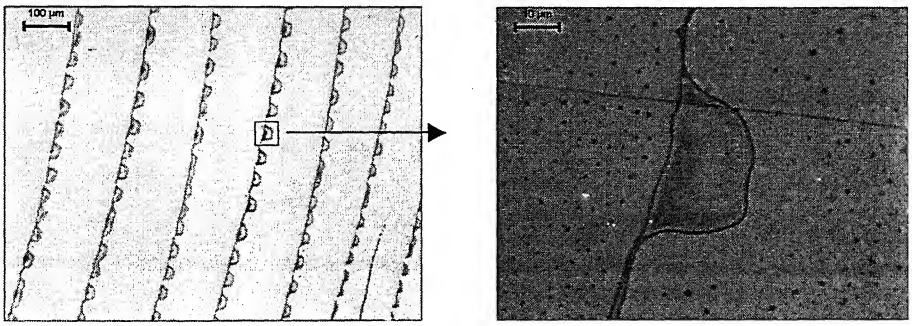

a b

Figure 3.17: Optical micrographs of the polymer ridges obtained during retraction of a solvent layer placed over a 30nm thick polystyrene film on silicon substrate at 20°C in presence of a 500 ml/m Nitrogen flow rate. On enlarging, (image b) polymer droplets are visible in between the ridges. Bar size are 100 µm and 10 µm for (a) and (b) respectively.

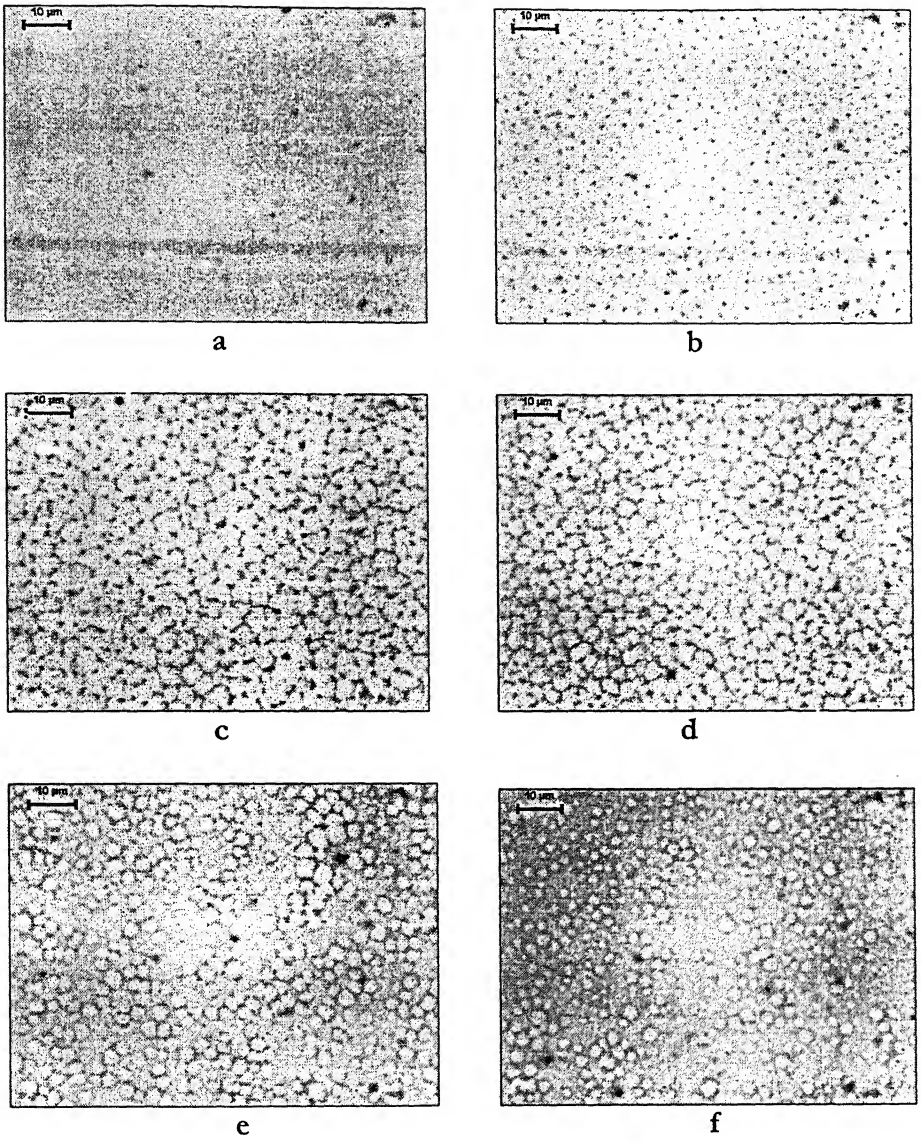

Figure 3.18: Optical micrographs of different features obtained, when a 1.0mm solvent layer placed over a 30nm polystyrene film on silicon substrate is allowed to evaporate in presence of a nitrogen flow of 500 ml/m. The images are at (a) 0.0mm (b) 1.0mm (c) 2.5mm (d) 3.0mm (e) 4.0 and (f) 4.5mm away towards the flow outlet from the centre. At the centre no features were observed. As we go towards the periphery polymer drops, Polygonal cellular structures and finally holes were observed. Bar size is 10 µm.

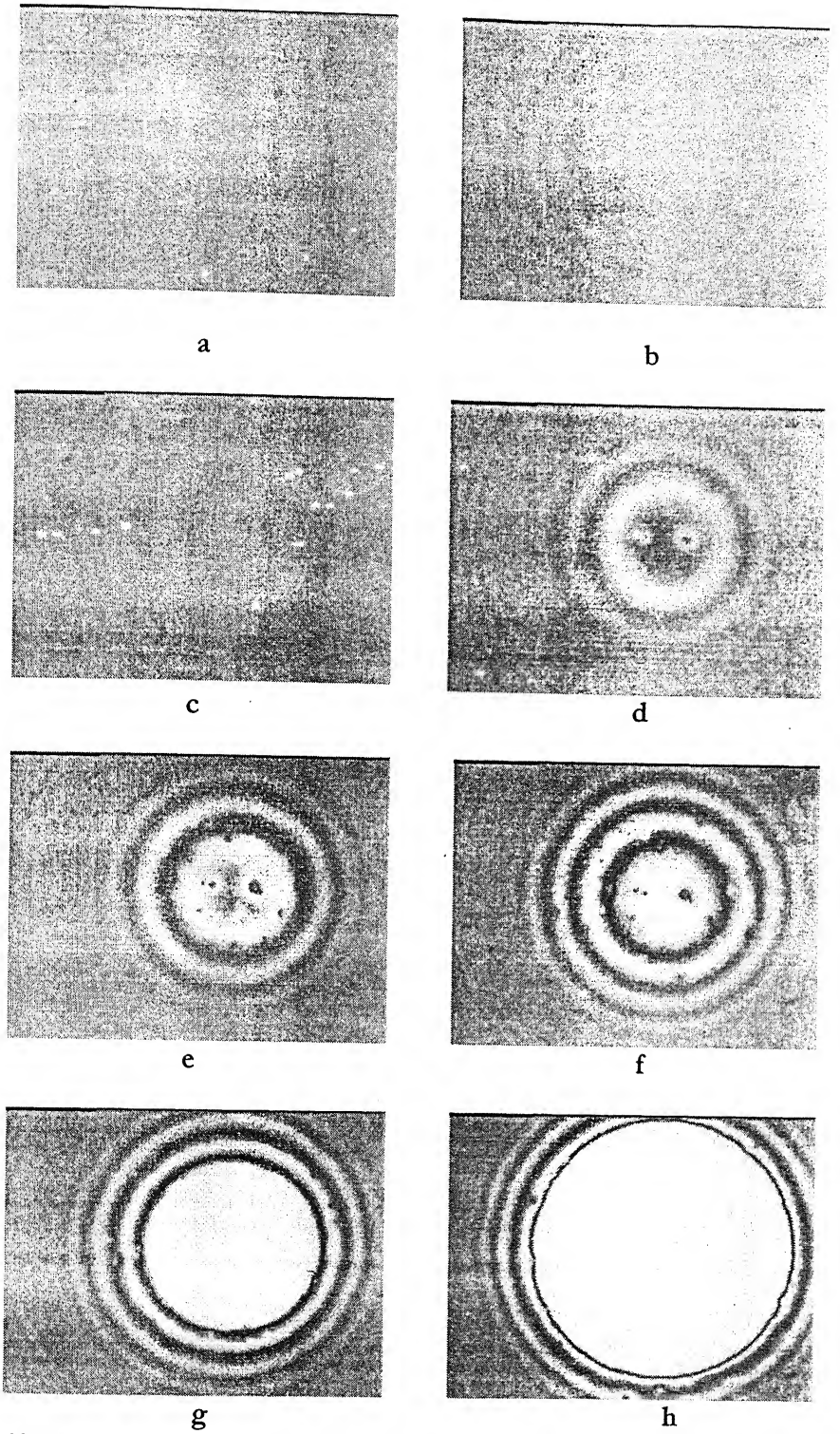

Figure 3.19: Rupture of a solvent film placed over a 30nm polystyrene film on silicon substrate at 20°C. The initial solvent layer was 1.0mm thick and it took 3 min and 40 sec minutes to rupture. The optical micrographs are taken (a) 0.0 sec. (b) 6.0 sec. (c) 8.0 (d) 10.0 (e) 11.0 and (f) 12.0 (g) 13.0 sec (h) 15.0 sec after the rupture of the film. Image size is 937 μm x 705 μm. Interference fringes are due to thickness variation.

At a lower nitrogen flow rate i.e. lower evaporation rate polymer droplets were seen at central region, which is not the case for higher nitrogen flow rate. As we go towards the periphery first the polymer ridges and then large polymer droplets arranged in a line were observed. All the structures are shown in figure 3.20. Surprisingly when there is no nitrogen flow and the solvent is allowed to evaporate covering with the lid (which produce a more or saturated atmosphere over the film) almost no features were observed. The film ruptured after 11 minute and 30 minutes under 200ml/min and 0 ml/min nitrogen flow rate respectively.

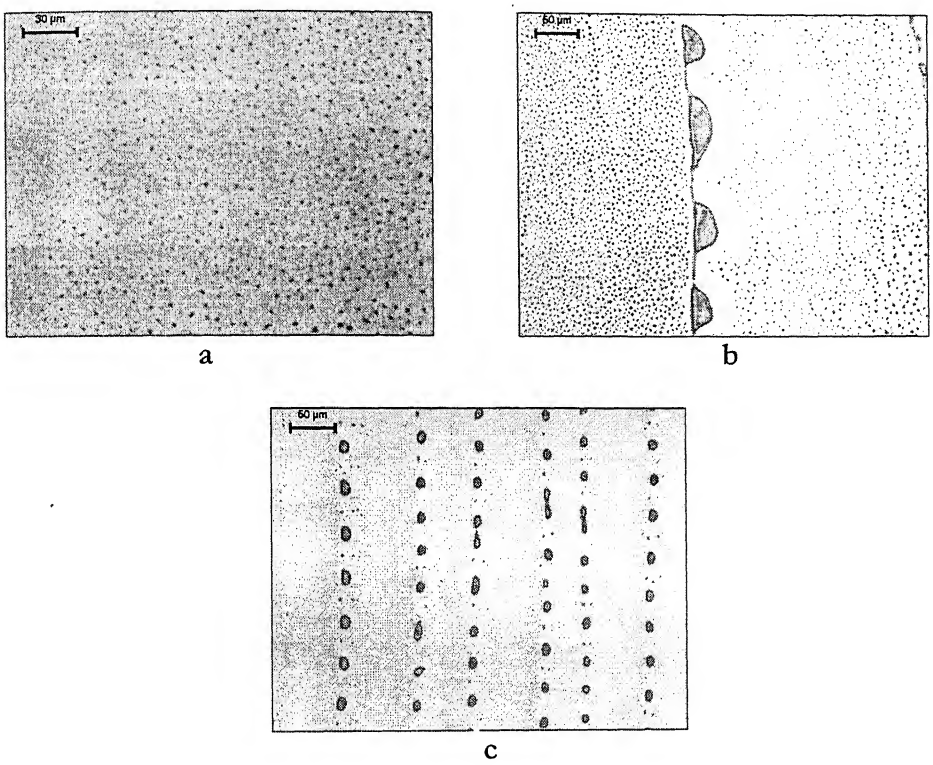

Figure 3.20: Optical micrographs of the features obtained when a 1.0mm solvent layer placed over a 30nm polystyrene film on silicon substrate is allowed to evaporate under a nitrogen flow of 200ml/m. Different features viz. (a) Polymer drops at the centre (b) polymer ridges away from the centre and (c) parallel array of polymer drops near the periphery are observed.

3.4.2 Evaporation of solvent (toluene) film placed over a thin (~45nm) polystyrene film coated on Quartz substrate:

Only a few experiments were done on Quartz substrates. On a 47nm film At 25°C, with a Nitrogen flowrate of 200 ml/min and 1050ml/min, polymer droplets are seen at the central region for both the cases. No density of polymer droplets is higher for higher flow rate. The time taken for initial rupture of film is 10 min 30 sec and 3 min 40 sec with 200 ml/min and 1050 ml/min nitrogen flow rate respectively.

At 15°C with 500 ml/min nitrogen flow rate at central region polygonal mesh structure disintegrating into droplets are seen while no features are seen with no nitrogen flow on a 45nm film.

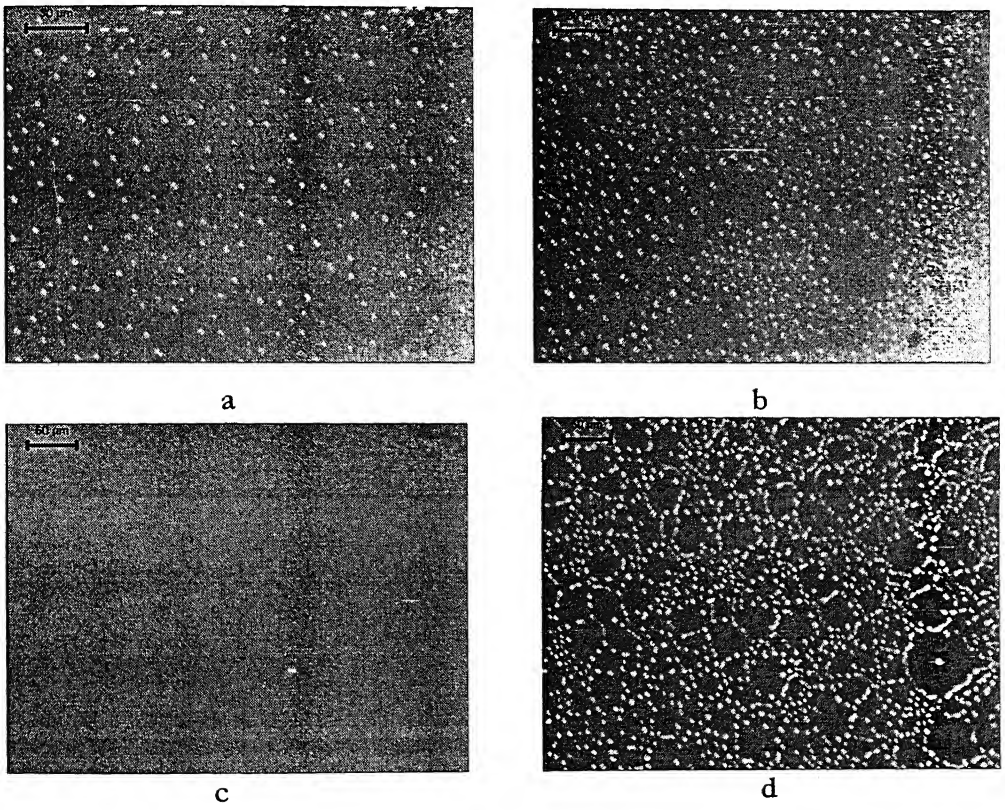

Figure 3.21: Optical micrographs of the features observed at the central region when a 0.7 mm solvent layer placed over a ~45nm polystyrene film on Quartz substrate is allowed to evaporate at 25°C (a and b) and 15°C (c and d) under different flow rate of nitrogen. Polymer droplets are seen for both the cases with 200ml/min (a) and 1050 ml/min (b) flow rate at 25°C. No features are observed with 0ml/min flow (c) and polygonal network disintegrating into droplets are seen with 500 ml/min flow (d) of nitrogen at 15°C. Bar size is 30 μm for a and b, while it is 50 μm for c and d.

At all temperature, towards the periphery parallel array of polymer droplets are seen to be produced during the retraction of three phase contact line. Images below show the formation of this ordered arrangement of polymer droplets from a retracting liquid layer for a 44nm thin polystyrene film with no nitrogen flow at 15°C.

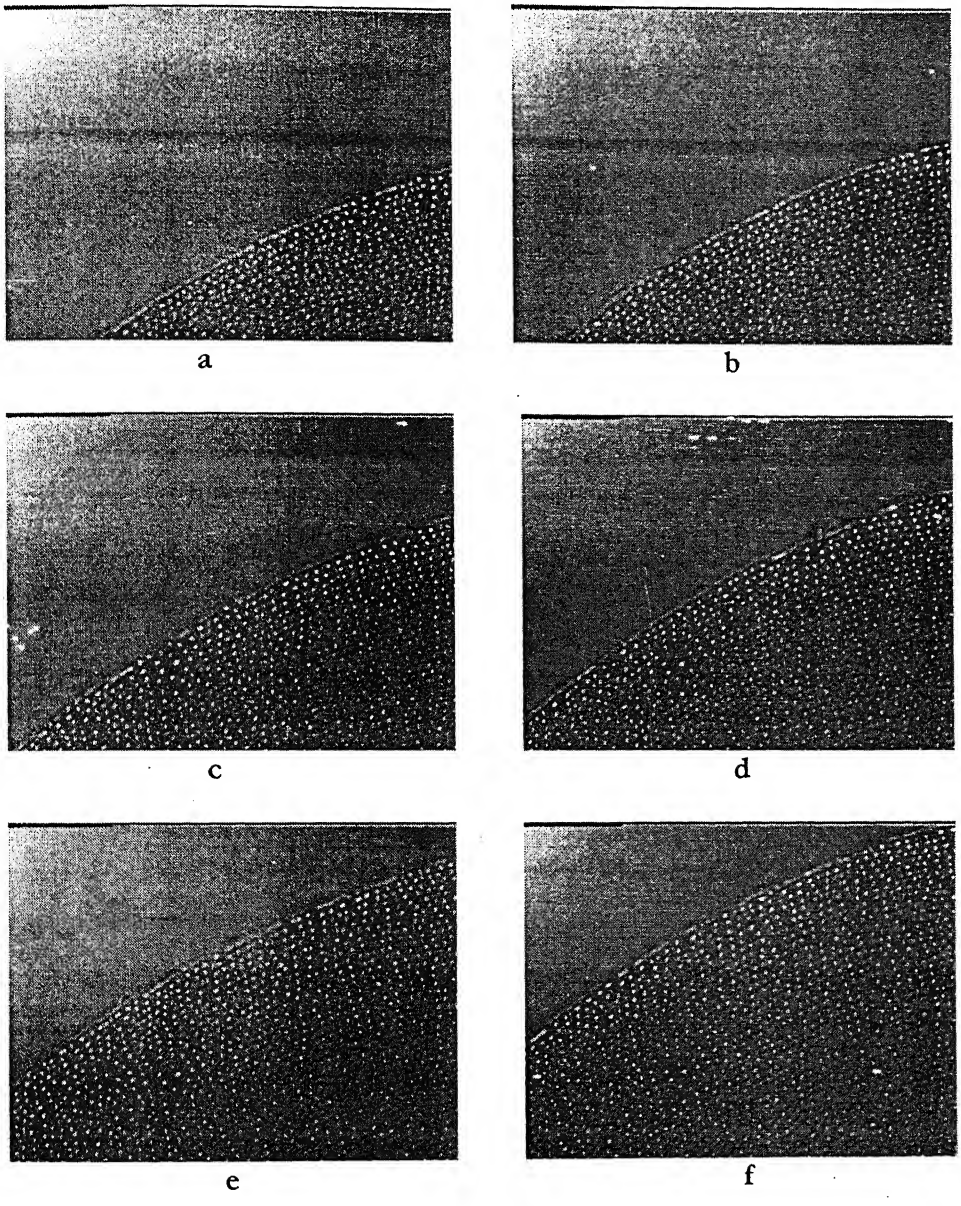

Figure 3.22: Optical micrograph of a sequence of formation of parallel array of polymer droplets during retraction of the liquid layer or three phase contact line. Images are taken at 16 seconds interval. The size of the images is 937 μm x 705 μm.

A QUALITATIVE DESCRIPTION OF THE PROCESS:

When a liquid solvent layer is placed over a thin polymer coated on glass, Quartz or silicon substrate bounded by a barrier, the upper layer takes a concave shape due to capillary forces. With time the solvent layer evaporates into the atmosphere and simultaneously the underlying polymer layer gets dissolved into the solvent. Depending upon the amount of solvent added, the rate of evaporation, thickness of the polymer film and rate of dissolution, the underlying polymer film may or may not dissolved fully into the solvent to expose the substrate. Typically after the addition of solvent the system can be divided into three zone, pure polymer layer on substrate, pure solvent layer near the top surface and a intermittent zone of solvent having dissolved polymer in it. The thickness of the different zone varies with time.

The reason behind different structures observed during (1) Rupture of film i.e the Central zone, (2) Stick-slip motion of the retracting liquid layer and (3) Continuous retraction of the liquid layer is discussed below.

At central region, it is observed that at all temperature (25°C and 20°C) polymer droplets are seen for 50 nm film while holes are observed for thicker (115nm and 230nm) films. For thin film the time is enough to dissolve the entire polymer at the centre to expose the substrate. The substrate being non-wettable for the solution when the liquid layer at the central region becomes thin, at some critical thickness it become unstable and ruptures to form droplets. The residual solvent evaporates to leaving behind the polymer dissolved in it which takes the shape of the droplets. For thicker film there is still a polymer layer left which is wettable to the solution. The solution film uniformly thins up to dry up at the centre. The holes are formed due to heterogeneous nucleation which has no time to grow at higher rate of evaporation, which is true for experiments done at 25°C. At relatively lower rate of evaporation, these holes have enough time to grow and coalesce to form polygonal structure and sometimes they even disintegrate to polymer droplets, which is true for experiments done at 20°C.

After the initial rupture and the retraction of the liquid layer, the three phase contact line gets pinned at the substrate. The rate of evaporation is highest along the contact as the liquid layer here is thinnest. So concentration of the polymer increases at the three phase contact line. With time the amount of solvent also decreases due to evaporation, so the volume of

liquid confined between the pinned line and barrier. After a time the capillary force overcome the frictional force due to pinning and the liquid layer detaches from the pinned line to retract further towards the periphery. The same process repeats and the liquid layer retract through stick-slip or pinning-depinning, leaving circular rims behind it at each pinned position. If the rate of evaporation is slow or the amount of polymer in the cylindrical rim is less, this rim disintegrates to form polymer droplets due to Rayleigh instability before dry up completely.

During continuous retraction of the film in between two pinned line polymer droplets are seen. This is due to the fingering instability of the 'bump' formed at the three phase contact line, which finally disintegrate into droplets.

Some preliminary results of the system studied have been reported. The structures obtained specially the parallel array of polymer dots are of significant importance technologically as a mean for production of ordered pattern in small scale. However the number of experiment done is not sufficient to quantify the process. More experiments have to be done with different solvent, different film material, at different nitrogen flow rate for a complete understanding of the process so that we can control the process according to our need.

CHAPTER 4

DEWETTING OF THIN POLYMER FILM IN SOLVENT VAPOUR ATMOSPHERE

4.1: Introduction:

Stability of thin films against dewetting has immense technological and scientific importance because of its widespread application in photo-resists, adhesives, lubricants and paints. Dewetting of thin (10-100nm) polymer film on solid substrates is widely studied theoretically [30-33] and experimentally [34-39]. In most of the cases dewetting is induced by annealing above glass transition temperature (T_g). A metastable or unstable polymer film can be coated on a nonwettable substrate by spin coating. When these films are annealed above T_g the mobility of the polymer chains increases and dewetting takes place through the sequence-initiation of holes with rims ,hole growth, coalescence of holes to form polygonal network structure and finally disintegration of this network into polymer droplets, in most of the cases. We have observed that dewetting of thin polymer films can be induced by the presence of solvent vapour. When a thin polystyrene film coated on Silicon substrate (having a native oxide layer of 2-3nm thickness) is exposed to solvent (toluene) vapour at room temperature the film dewets the substrates. The process of dewetting induced by solvent vapour is monitored for thin (<50nm) films. The influence of film thickness on the process and various characteristic features viz. hole density (N_H), polygon diameter (D_p), average drop size (D_d), and drop size distribution is investigated and is compared with the present theory for temperature induced dewetting.

4.2: Experimental section:

Polystyrene [MW 280000, Glass transition temperature (T_g): 100°C] was deposited by spin coating from HPLC grade toluene solution onto a 1cm x 1.5cm silicon substrate with a native oxide layer of 2-3nm thick. By changing the concentration and spin speed we were able to prepare film of thickness 10-50nm [see Sec. 2.1.3]. Polystyrene was dissolved in toluene and heated a little to dissolve it quickly. Then the solution was filtered through a 0.22 μm filter to remove any dust particle. Then this solution was used for coating films. The silicon substrates were thoroughly cleaned before coating in the procedure described in the sec. 2.1.2. Coating was done within a class 100 clean bench. After coating the films were

stored under vacuum for 24 hours to remove any residual solvent. Then the films were annealed at 60°C for 6 hours to remove any strain that might have developed during the non-equilibrium spin coating process. The annealed film were quenched at room temperature (25°C) and stored under vacuum. Now films were ready to be used in the experiment. Film thicknesses were measured by nulling ellipsometry.

The films were exposed to toluene vapour in two different ways. First enough amount of HPLC grade toluene was kept in a dessicator for over an hour so that the dessicator became almost saturated with toluene vapour at operating temperature i.e. 25°C. Then PS films were kept inside the desiccator and were covered as quickly as possible to decrease loss of toluene vapour in atmosphere. The PS films were kept like this for different time, removed and dried under vacuum for 30 minutes to remove any residual solvents. The samples were then examined under optical microscope. The schematic and the actual arrangement are shown in figure 4.1 and 4.2 respectively.

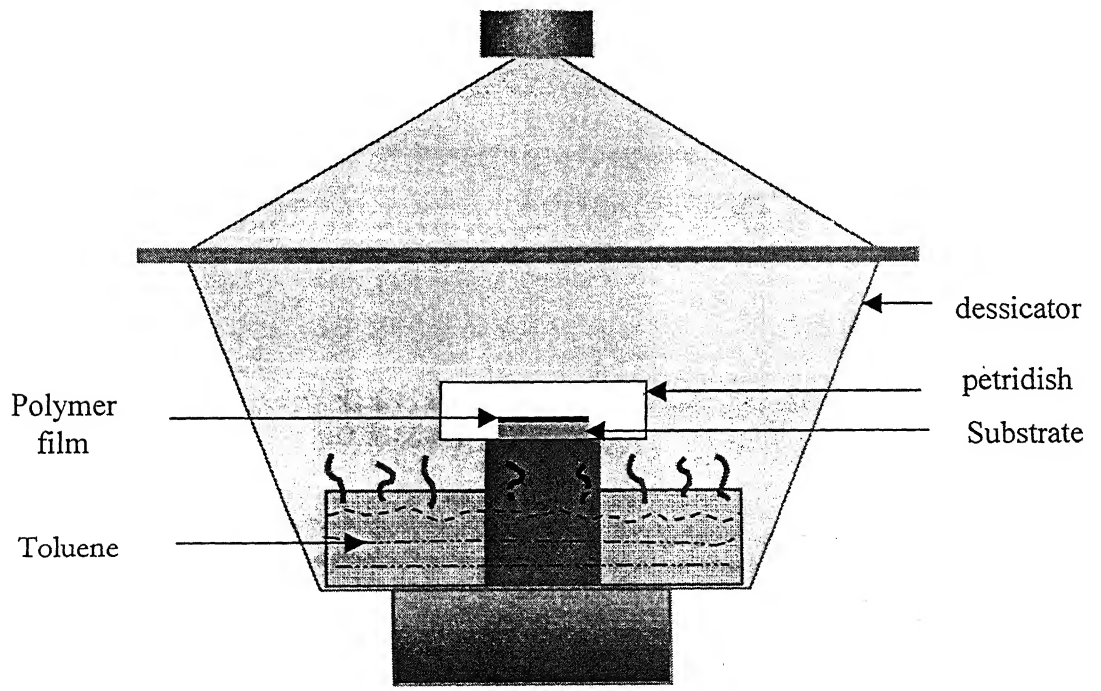

Figure 4.1: Schematic of the arrangement where the polystyrene film is exposed in solvent vapour within a dessicator. Solvent (toluene) is kept in a petridish at the bottom and polymer film is kept above it on a stand within a small petridish.

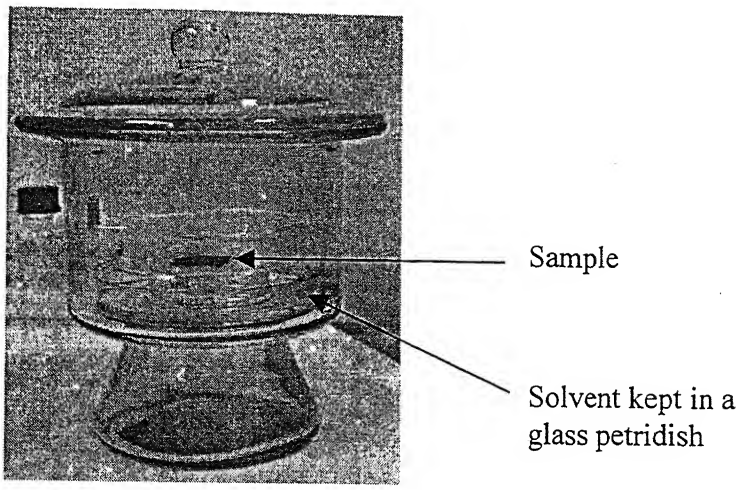

Figure 4.2: Actual arrangement where the polystyrene film is exposed in solvent vapour within a dessicator.

But in this arrangement it was not possible to examine the process in situ. Also few experiments need to be done at lower temperature (0°C). For these, experiments were done in a heating stage keeping toluene in small Teflon crucible inside it. The temperature inside the heating stage can be controlled by circulating liquid with the help of a refrigerator-recirculator through it. The only problem was, due to lack of space, toluene has to be kept at one point only which made the toluene vapour concentration different at different region. So the dewetting was not uniform at all the places of the films. This problem was not very prominent with the experiments done in the desiccator where the atmosphere is more uniform.. The heating stage used for the experiment is shown below.

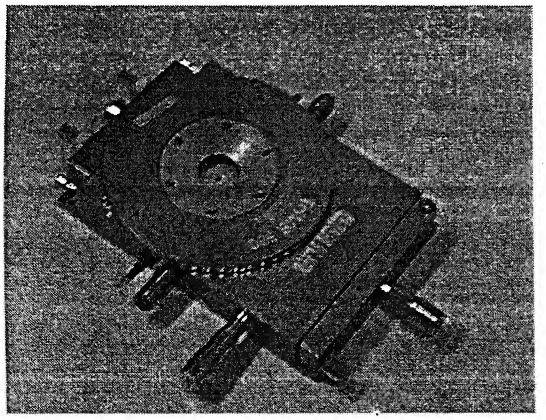

Figure 4.3: Heating Stage used for experiments at low temperature.

4.3 Results and Discussions:

4.3.1 How dewetting is induced by solvent vapour?

Glass transition temperature (T_g) is a temperature below which amorphous polymers becomes hard and brittle, remains in the glassy state, in which the polymers chains are not allowed to move freely. Above this temperature they are known to be in rubbery state and become soft and flexible. The polymer chains become mobile. So when a metastable thin polymer film is heated above the glass transition temperature dewetting takes place.

Now this glass transition of polymer film can also be induced by solvent vapour. According to Leibler and Sekimoto [40], due to the elastic properties, the polymer film in glassy state has the capability to absorb gas or liquid present in the surrounding. When the polymer film is placed in the solvent vapor, the polymer film swells up by the adsorbed solvent gas gradually, which leads to the increase of the free volume (V_f) of the polymer. It means the decrease of T_g of polymer/solvent film with the following absorption of the solvent vapor, i.e., the glass transition temperature of polymer/solvent film solution decreases as the solvent concentration increase. Consequently, the glass transition occurrence of the polymer/solvent film depends both on the temperature and on the concentration of the solvent vapor absorbed in the film. Take the solvent sorption into account, the glass transition temperature decreases below the T_g of bulk dry polymer material.

We observed dewetting of polystyrene film in presence of saturated toluene vapour at room temperature (25°C) and also at 0°C. The glass transition temperature for bulk polystyrene is 100°C. So the question arises is if it is possible to decrease the glass transition temperature for polystyrene below 0°C in presence of solvent vapour?

When thin polystyrene film is exposed in saturated toluene atmosphere, it swells up through the adsorption of gas solvent due to the elastic properties of its glassy state. So the free volume of polymer and consequently the chain mobility increases. With the increase of amount of gas solvent adsorbed the glass transition temperature of the polymer/solvent (PS/toluene), $T_{G/PS}$ decreases.

According to Leibler and Sekimoto's models, [40] the activity versus solvent content in the film in the glassy domain could be got by the following equation:

$$a = P_{SV}/P_{SVO} = (1 - \Phi_P)\exp[\Phi_P + \chi \Phi^2_P - v_S K/RT \ln(\Phi_P / \Phi_{PG}(T))] \quad \ldots 4.1$$

where *a*, the activity, is the ratio of the saturated vapor pressure of the solvent in equilibrium with solution (P_{VS}) to the saturated vapor pressure of the pure solvent (P_{VSO}). Φ_P is the polymer volume fraction. Φ_{PG} ($\Phi_{PG} = 1 - \Phi_{SG}$, Φ_{SG} is the solvent volume fraction, at which glass transition of polymer/solvent occur) is the polymer volume fraction at which glass transition took place. χ is the Flory-Huggins interaction parameter which represented the affinity between the polymer and the solvent. v_S is the solvent molar volume. *K* is the bulk modulus that is assumed to be constant in the glassy domain. T is the experimental temperature and R is the perfect gas constant. Combining the experiment data with equation (1) given by Leibler and Sekimoto's models, the polymer volume fraction at the glass transition Φ_{PG} at the experimental temperature could be estimated.

For a given Φ_{PG} the glass transition temperature for a polymer/solvent ($T_{G/PS}$) can be calculated by a equation proposed be Kelle and Bueche [41]

$$T_{G/PS} = [c\, \Phi_{PG}\, T_{G0} + \alpha_S (1 - \Phi_{PG}) T_{GS}]/[c\, \Phi_{PG} + \alpha_S (1 - \Phi_{PG})] \quad \ldots\ldots 4.2$$

Where $c = 4.8 \times 10^{-4}\ K^{-1}$, $\alpha_S = 10^{-3}\ K^{-1}$, T_{G0} is the glass transition temperature of the dry polymer and T_{GS} is the glass temperature of the solvent.

For our case the polymer was polystyrene and solvent was toluene. We were not able to measure the Φ_P at different pressure, so the Φ_{PG}. Instead from the equation 2 we plot $T_{G/PS}$ vs Φ_{PG} to see the effect for our system. Considering T_G for bulk polystyrene as 100°C and T_{GS} for toluene is 117 K [42] the variation is shown in the figure 4.4. We tried dewetting below room temperature upto 0°C. Dewetting occurs for all the cases. It is clear from the graph that $T_{G/PS}$ is lower than 0°C for Φ_{PG} lower than 0.75. ($T_{G/PS}$ value is 268 K (-5°C) at $\Phi_{PG} = 0.75$). So if Φ_{PG} is decreased below 0.75 when Polystyrene is exposed in saturated toluene vapour, the $T_{G/PS}$ for polystyrene/toluene system can decrease below 0°C and dewetting could take place.

Glass transition temperature ($T_{G/PS}$) Vs polymer volume fraction (ϕ_{PG})

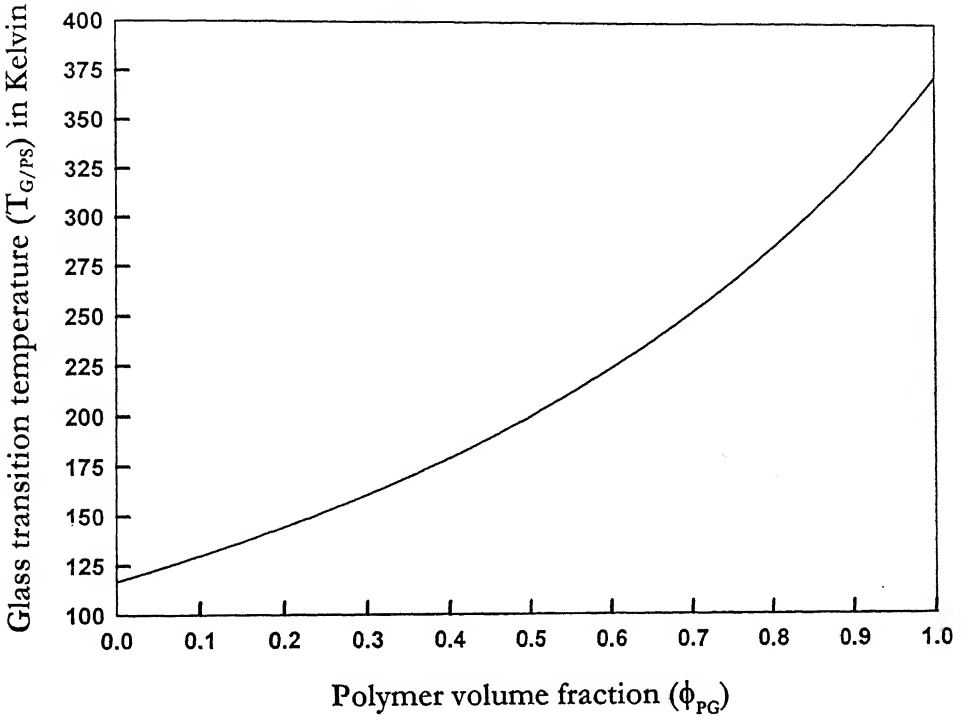

Figure 4.4: The variation of effective glass transition temperature ($T_{G/PS}$) for a Polystyrene/adsorbed toluene system with polymer volume fraction (Φ_{PG}).

4.3.2 Evolution of the structure with time:

Figure 4.5 and 4.6 shows the different stages of dewetting for an 18.84nm and 16.29nm thick polystyrene film from silicon substrate. The optical micrographs are taken at different time interval after exposing the film in saturated solvent atmosphere in a chamber. The experiment was done at 25°C. Almost similar to the temperature induced dewetting, here also dewetting took place through rupture of film by random hole formation, hole growth and coalescence, formation of polygonal cellular pattern and finally disintegration of polymer ridges into spherical droplets. These four stages of dewetting are distinctly visible for 18.84nm film. Rupture of film through formation of holes (a-b), hole growth and coalescence (c-d), polygonal cellular structure (e-f) and disintegration of polygonal ridges into droplets (g-h) are observed. For 16.29nm thick film the different phases are not that distinctly separable. The holes are less circular and the rims of the growing holes have undulations.

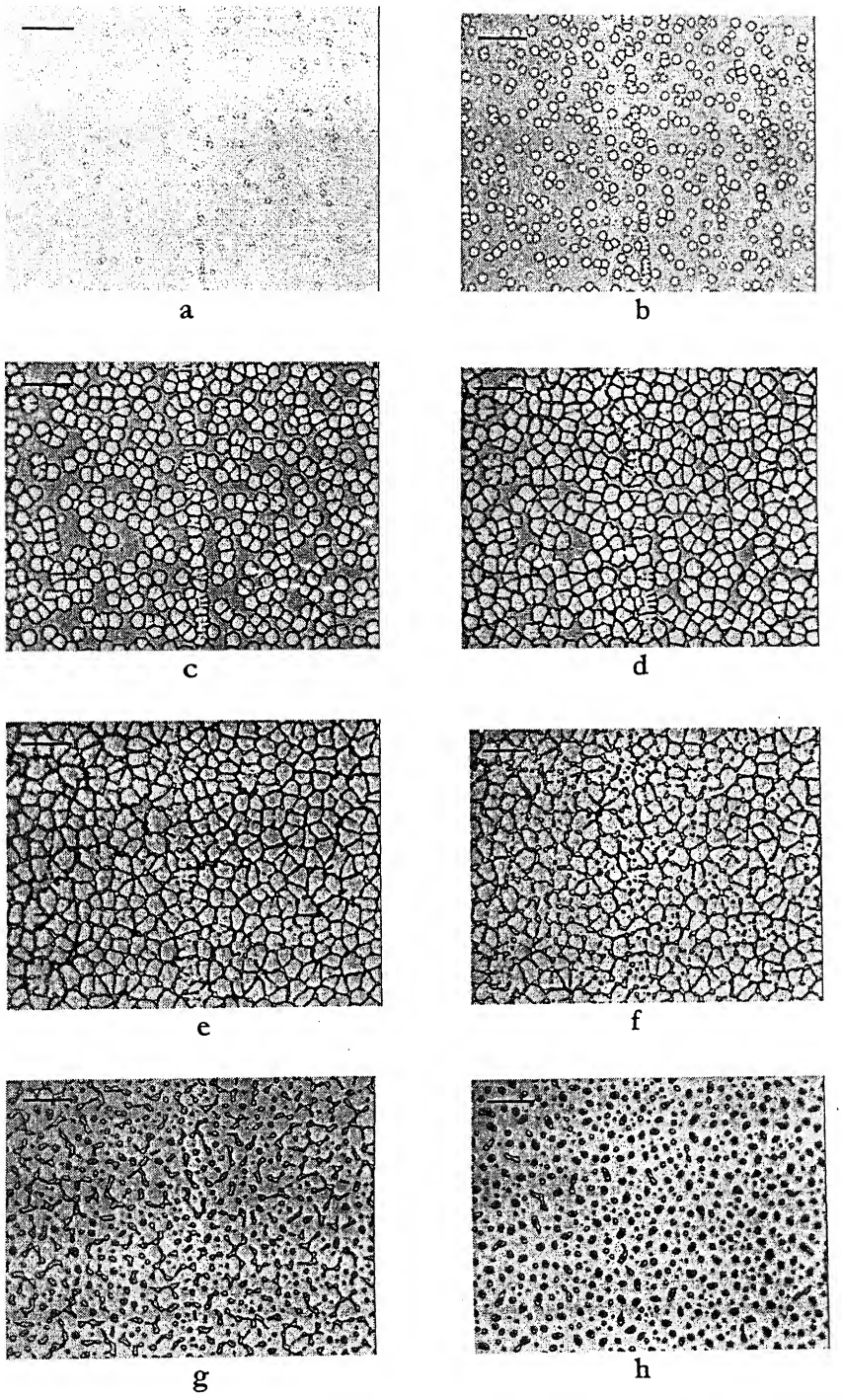

Figure 4.5: Different stages of dewetting induced by solvent (toluene) vapour for a 18.84nm thick polystyrene film coated on Si substrate. These are optical micrographs taken a. 5.5 min. b. 9 min. c. 15min. d. 20min. e. 30min f. 40 min. g.60 min and h. 120 min after exposing them into solvent vapour kept in a chamber at 25°C. Initiation of holes (a-b), hole growth and coalescence (c-d), polygonal cellular structure (e-f), and formation of polymer droplets (g-h) are seen. The bar size is 30 microns.

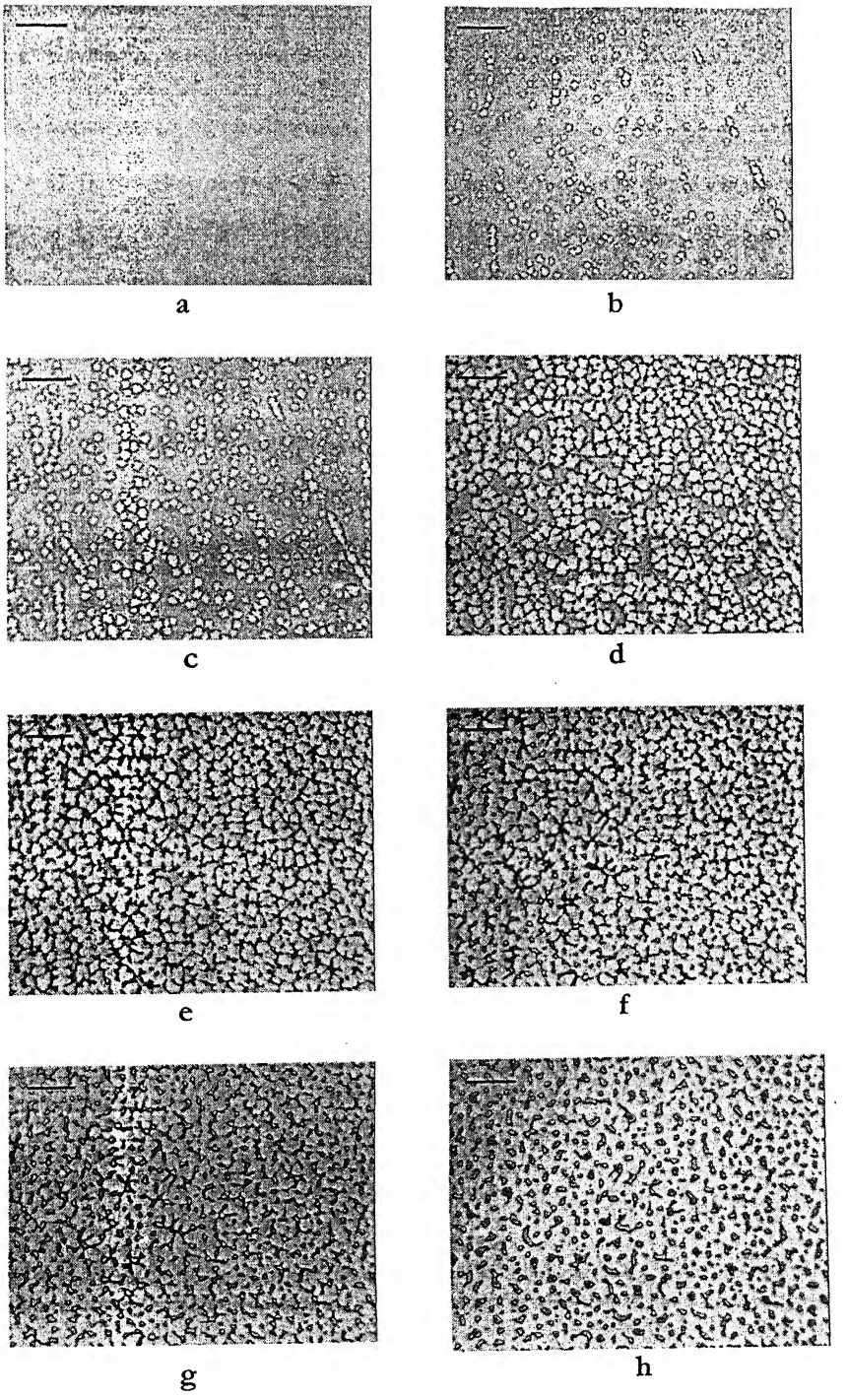

Figure 4.6: Different stages of dewetting induced by solvent (toluene) vapour for a 16.29nm thick polystyrene film coated on silicon substrate. These are optical micrographs taken a. 10 min. b. 15 min. c. 20min. d. 30min. e. 40min f. 50 min. g. 60 min and h. 120 min after exposing them into solvent vapour kept in a chamber at 25°C. Initiation of holes (a-b), hole growth and coalescence (c-d), polygonal cellular structure (e-f), and formation of polymer droplets (g-h) are seen. The bar size is 30 microns.

4.3.3 Dewetted structures, characteristics and variation with film thickness:

Films of thickness viz. 12nm, 20nm, 30nm, 50nm were exposed to solvent vapour to see the effect of thickness on the dewetting process. Figure 4.7 shows the final dewetted patterns formed 5 hours after exposing them in saturated solvent atmosphere. For all thickness the final structures formed from dewetted polymer film were spherical polymer droplets. Visually no specific orientation of the polymer droplets is seen and they seem to be quite random. The average drop size (D_d) increases with film thickness, although there is a wide size distribution of droplets for a particular thickness. Fast fourier transform of the optical micrographs reveals that there is a dominant wavelength (λ_d) present which increases linearly with film thicknesses. The no density of the holes (N_H), formed initially before coalescence, and the polygon diameter (D_p) were determined. The representative images based on which these calculations were done is given in figure 4.8. The variation of these parameter i.e mean equivalent diameter (D_d) of polymer droplets, no density of holes (N_H), Polygon diameter (D_p) etc. with film thickness is described in the following section.

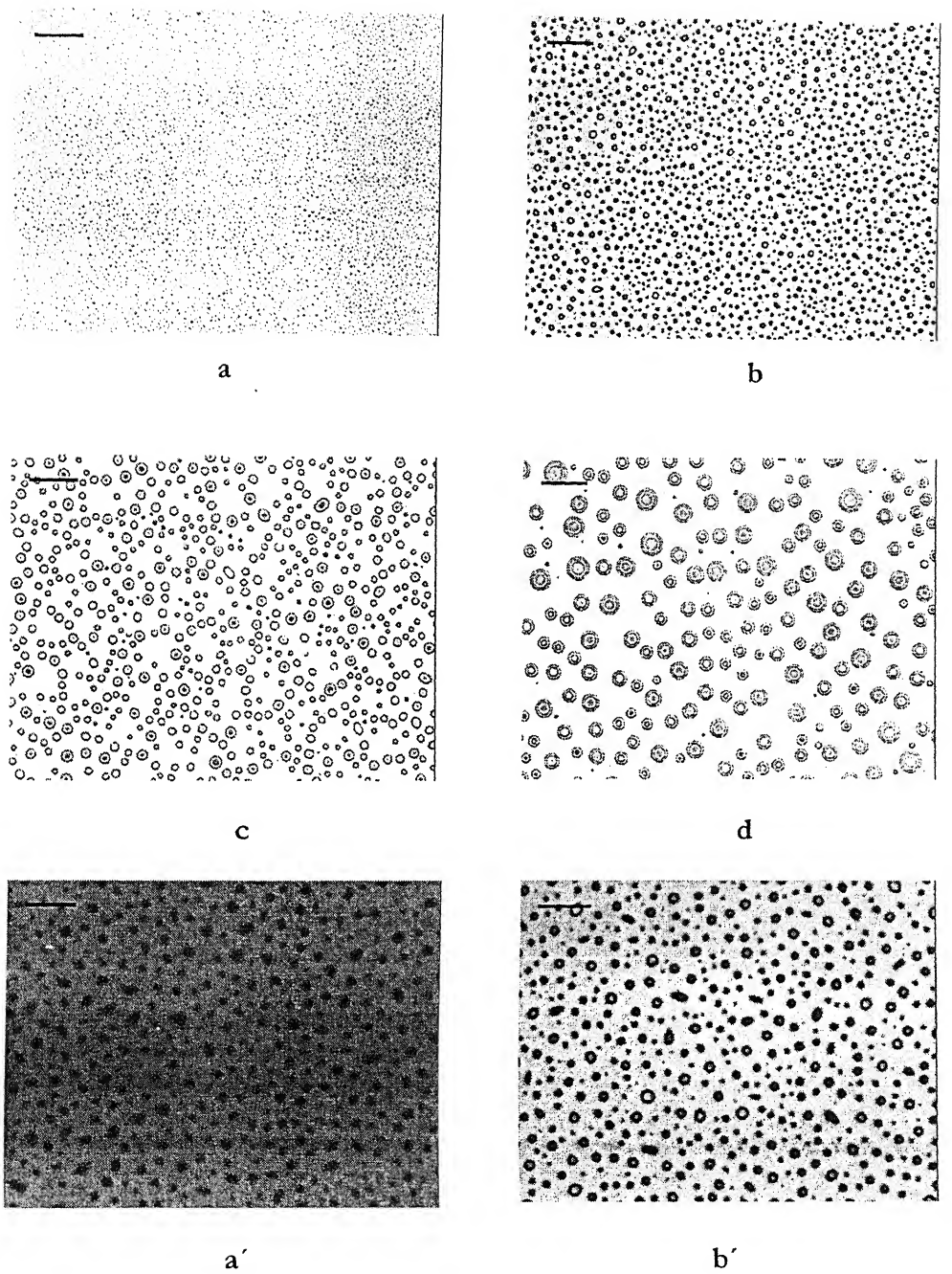

Figure 4.7: Optical micrographs of final dewetted patterns for a 12nm (a and a´), 20nm (b and b´), 30nm (c), and 50nm (d) polystyrene film on silicon substrate after 5 hours of exposure in solvent (toluene) vapour at 25°C. The bar size is 50 microns for a, b, c, and d. For a´ and b´ bar size are 10 microns and 30 microns respectively.

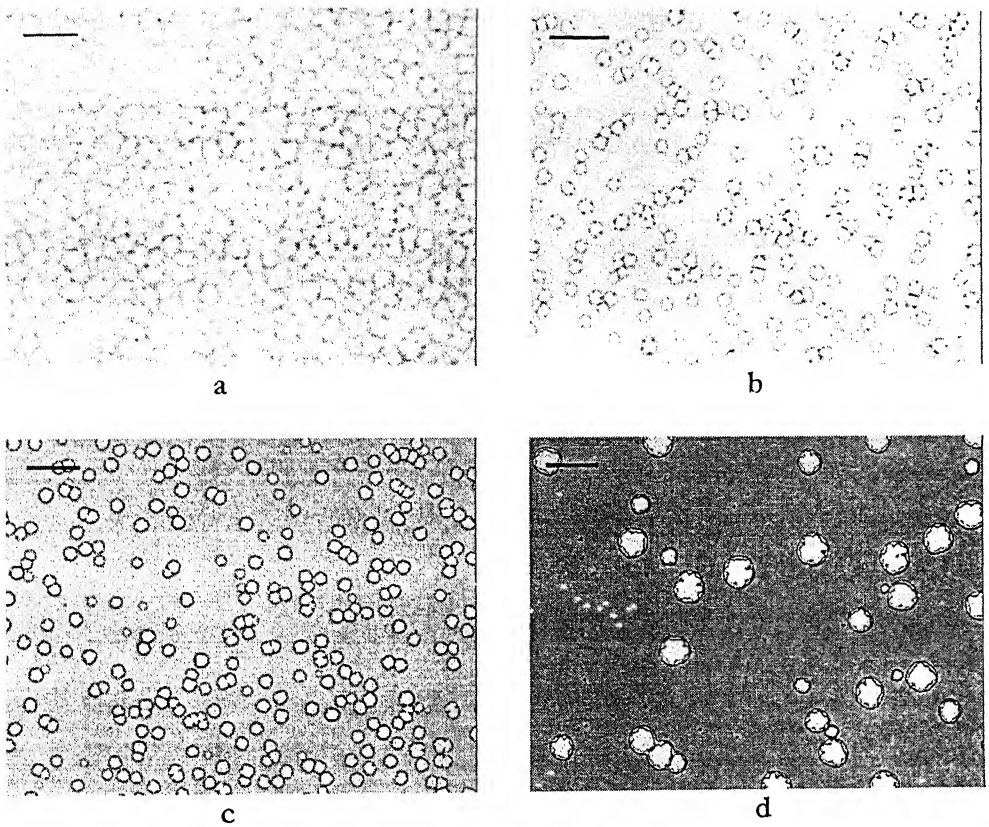

Figure 4.8: Representative optical micrographs of partially dewetted films for a. 12nm b. 20nm c. 30nm d. 50nm thick polystyrene film coated on silicon wafer used for calculation of maximum hole density. The bar size are 10μm, 30μm, 50μm and 100 μm for image a, b, c and d respectively. Experimental temperature is 25°C.

The variation of average number of holes per 100000 μm^2 (N_H) with film thickness (h) is seen in figure 4.9. The best linear fit to the data for all thicknesses on double logarithmic plot gives $N_H \propto h^p$ where p is – 4.9. If we consider only the smaller thicknesses (<30nm) the best fit p value is -3.8.

a.

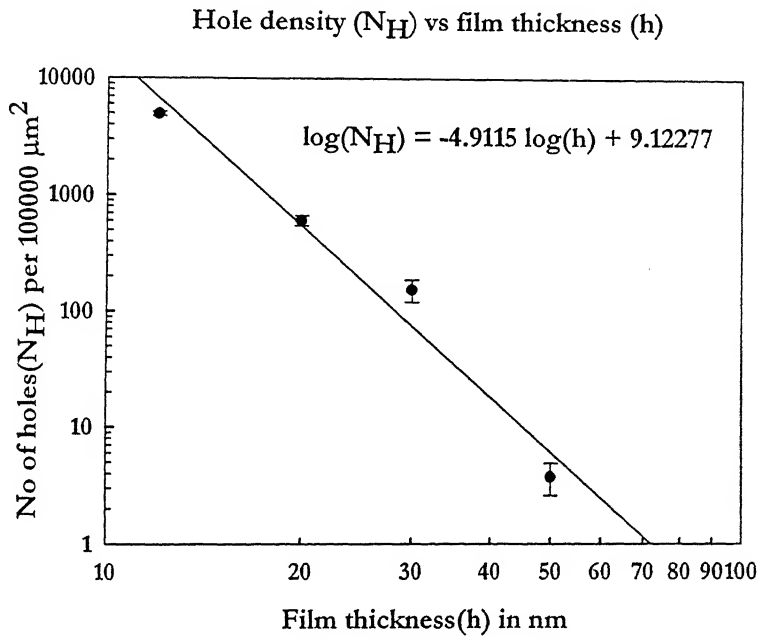

b.

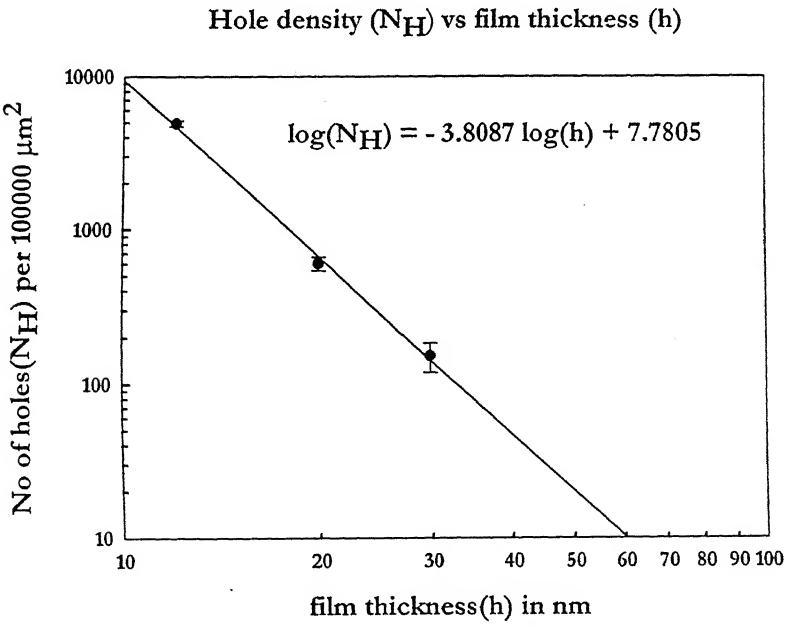

Figure 4.9: Dependence of hole density on film thickness for a. all data range and b.small thickness (upto 30nm).

Now in theory the no of holes formed per unit reference area (N_H) is related to excess free energy as

$$N_H = \lambda^{-2} = 1/8\pi^2\gamma\,(-\frac{\partial\varphi}{\partial h}) \quad \text{.....4.3}$$

Where, λ is the wavelength of the fastest growing mode, γ is the surface tension of the film and φ is the excess interaction potential or van der Waals potential. Now a general expression for van der Waals potential considering both the retarded and non retarded part is given by Kargupta *et al.* [43] as

$$\varphi = A(1 + c_1h/R) \,/\, [6\pi h^3(1 + c_2h/R)^2] \quad \text{.....4.4}$$

where A is the Hamaker constant, and R is a retardation parameter, c_1 and c_2 are numerical constants, taken as 7.98 and 5.32 respectively. For thin films $h/R << 1$ and φ approaches the non retarded van der Waals potential $\varphi \sim A/6\pi h^3$. Increasing the film thickness increases the effect of retardation and $\varphi \sim (c_1/c_2^2)\, AR/6\pi h^4$.

So for thin films ($h/R << 1$) when only non retarded van der Waals potential is dominant,

$$N_H \sim A/16\pi^3\gamma h^4 \quad \text{.....4.5}$$

And considering retardation for higher thickness

$$N_H \sim c_1AR/12c_2^2\pi^3\gamma h^5 \quad \text{.....4.6}$$

In our experiment considering only the smaller thicknesses (first three thickness upto 30nm) the exponent is coming -3.8, while taking the data for 50nm film exponent is shifted to -4.9 which agrees with the predicted value of -4 and -5 from equation 4.5 and 4.6 respectively.

If we consider only the non retarded van der Waals potential, from equation 5, Hamaker constant (A) for the system is given by,

$$A = N_H \times 16\pi^3\gamma h^4 \quad \text{.....4.7}$$

Where $\log(N_{11}) = -3.8087 \log(h) + 7.7805$, taking film surface tension $\gamma = 29.35$ mN/m which is the arithmetic mean of surface tension of polystyrene, 30.8 mN/m and surface tension of toluene 27.9 mN/m, effective Hamaker constant (A) for the system air/PS/SiO is calculated using equation 4.7. It is found to be 1.54 E^{-20} Joules which is in agreement with the Hamaker constant calculated by the refractive indices and di-electric constant of the materials in layered system air/PS/SiO, A = 1.8 E^{-20} Joules.

The variation of polygon diameter (D_p) with film thickness (h) is shown in figure 4.10. The best linear fit of all data on a log-log plot gives the slope as 2.48 and considering only the first three points gives the slope as 1.92. Now Sharma and Reiter [44] shows that the polygon diameter (D_p) is related with film thickness as

$$D_p = (4h^2/d_0)\,[-N_C \pi \gamma / 3 S^{LW}]^{1/2} \quad \ldots\ldots 4.8$$

i.e $D_p \alpha h^2$

So our experimental findings agree with the theoretical prediction.

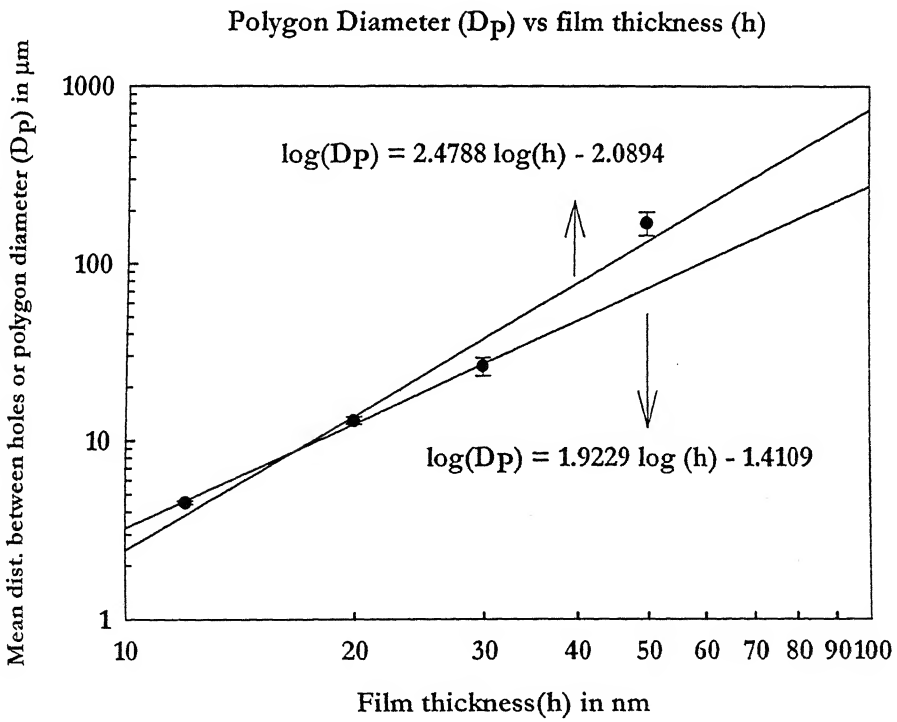

Figure 4.10: Variation of polygon diameter (D_p) i.e the distance between the holes, with film thickness

The variation of mean equivalent diameter of the polymer drops formed after dewetting with film thickness is shown in figure 4.11. The best linear fit on a log-log plot gives the slope as 1.547. Sharma and Reiter [44] shows that the diameter (D_d) of the spherical drop formed from polygonal edges due to Rayleigh instability is

$$D_d^3 = 24\sqrt{2}\,(D_p h n_f)^{3/2}\,\theta\,\sin^3\theta[(2+\cos\theta)\times(1-\cos\theta)^2\,(2\theta-\sin 2\theta)^{1/2}]^{-1} \quad \ldots\ldots 4.9$$

Where D_p = diameter of the polygons given by equation 4.8, n_f the fraction of original mass collected in the polygonal edges (between two polygonal holes) and θ is the contact angle of the film material on substrate. Combining equation 4.9 and 4.8 we get $D_d \propto h^{3/2}$. So our experimental findings $D_d \propto h^{1.54}$ agree with the theoretical prediction.

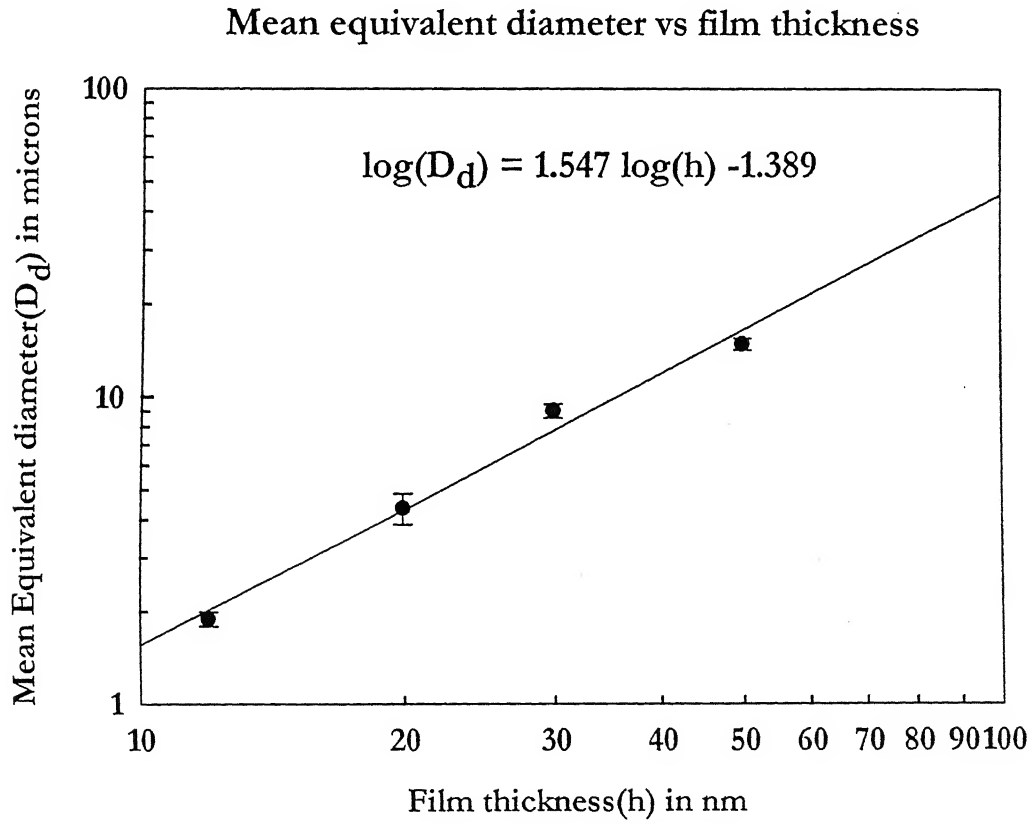

Figure 4.11: Variation of mean equivalent diameter (D_d) of the polymer drops with film thickness (h).

Doing Fast Fourier Transform of the final structures we have found that there is a dominant wavelength, which increases linearly with the film thickness. The variation is shown in figure 4.12.

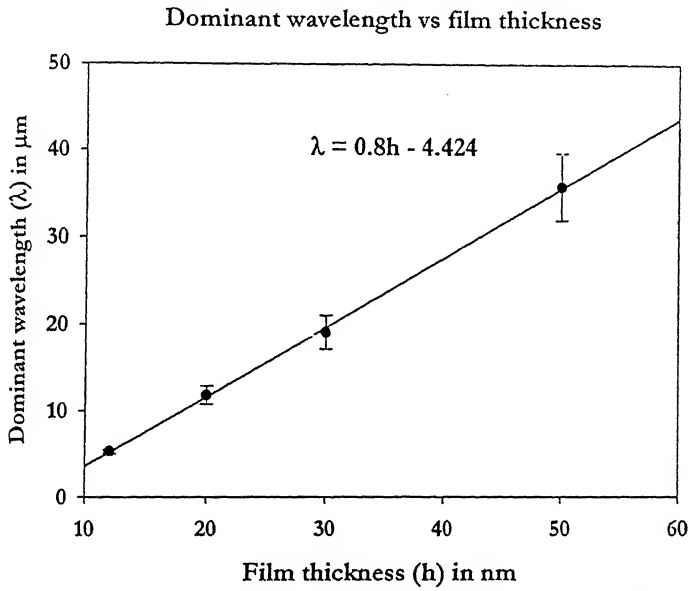

Figure 4.12: Variation of dominant wavelength found from FFT of the structures formed after complete dewetting, with film thickness.

Variation of no of polymer drops (N_D) formed per 10000 μm^2 with film thickness is shown in figure 4.13. The best linear fit on a log-log plot gives the slopes as -2.835. So $N_D \alpha h^q$ where $q = -2.835$.

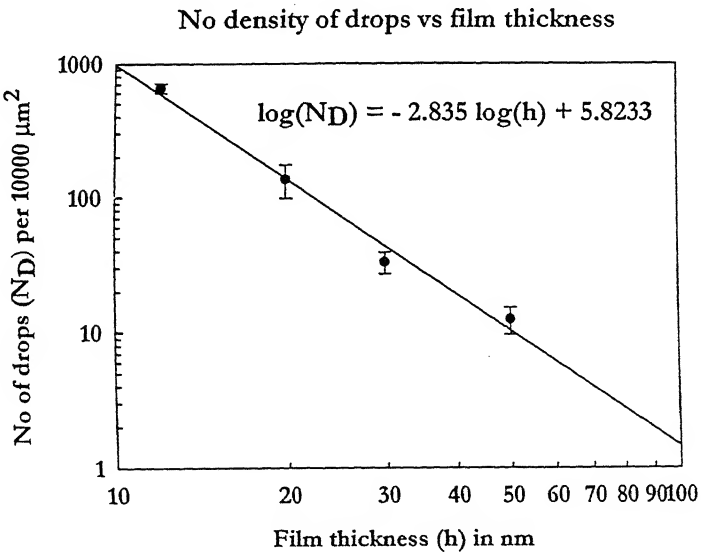

Figure 4.13: Variation of no of polymer droplets per 10000 μm^2 with film thickness.

The size distribution of polymer drops formed after dewetting is shown in figure 4.14 and 4.15. It is observed that for small thicknesses, 12nm and 20nm, dropsize is distributed over a single maxima, while for 30nm and 50nm film two distinct dominant dropsize is observed. This may be due to bimodal dewetting, which is dominant for higher thickness.

a.

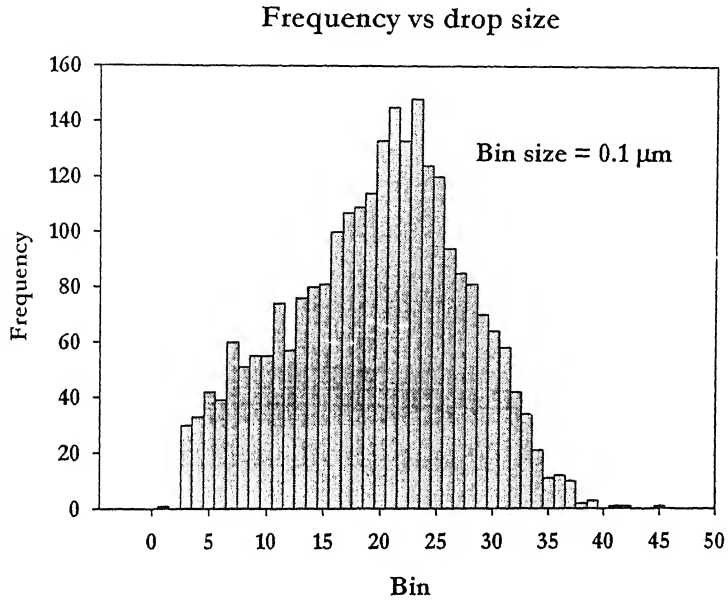

b.

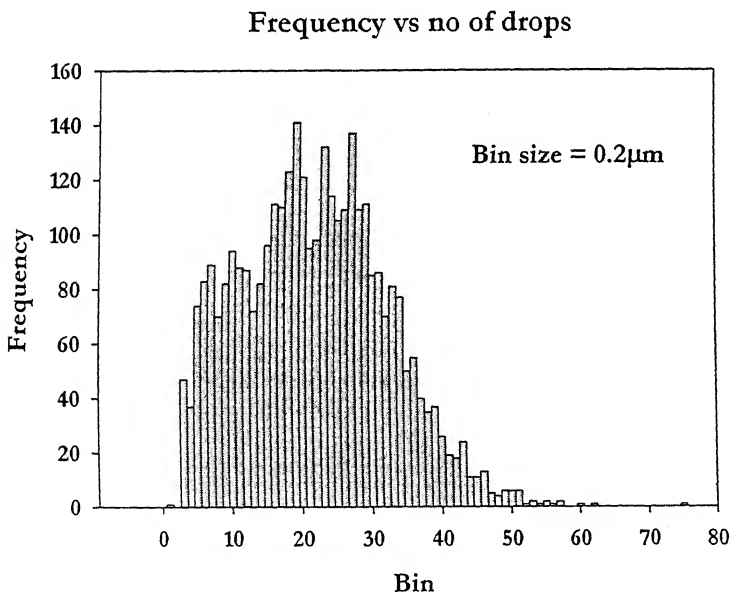

Figure 4.14: Drop size distribution for a. 12nm and b. 20nm thick film.

a.

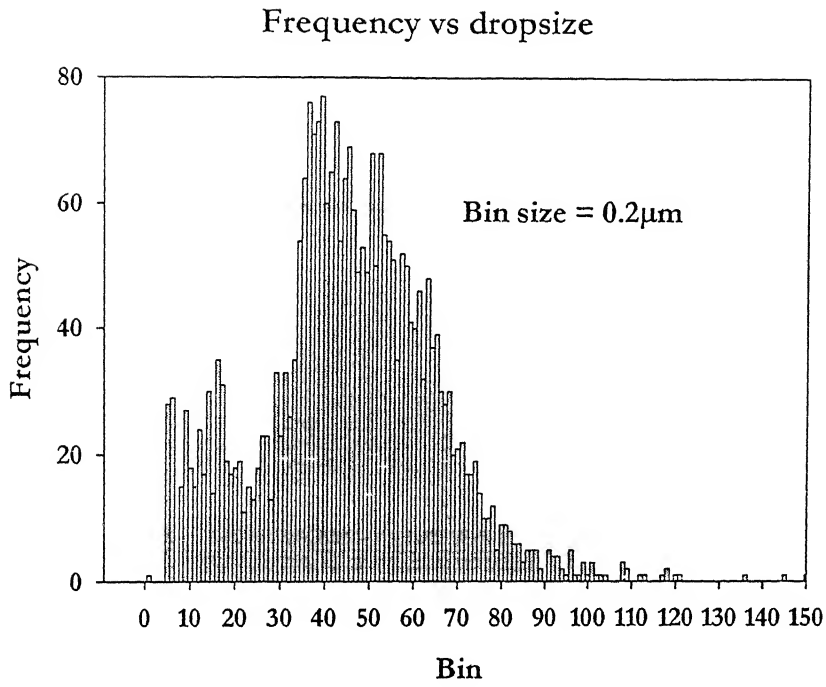

b.

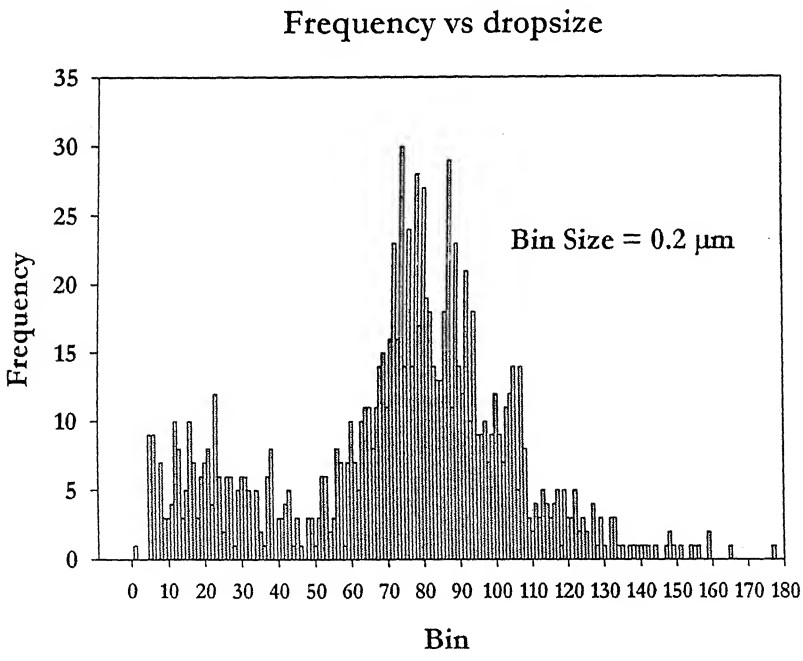

Figure 4.15: Drop size distribution for a. 30nm and b. 50nm thick film.

We have done few experiments with polystyrene film coated on Quartz substrate. Dewetting is observed when exposed to solvent vapour for this case also. The final dewetted structures of the polymer films after six hours of exposure in solvent atmosphere are shown below. The characteristic features are almost similar to the film coated on silicon wafer.

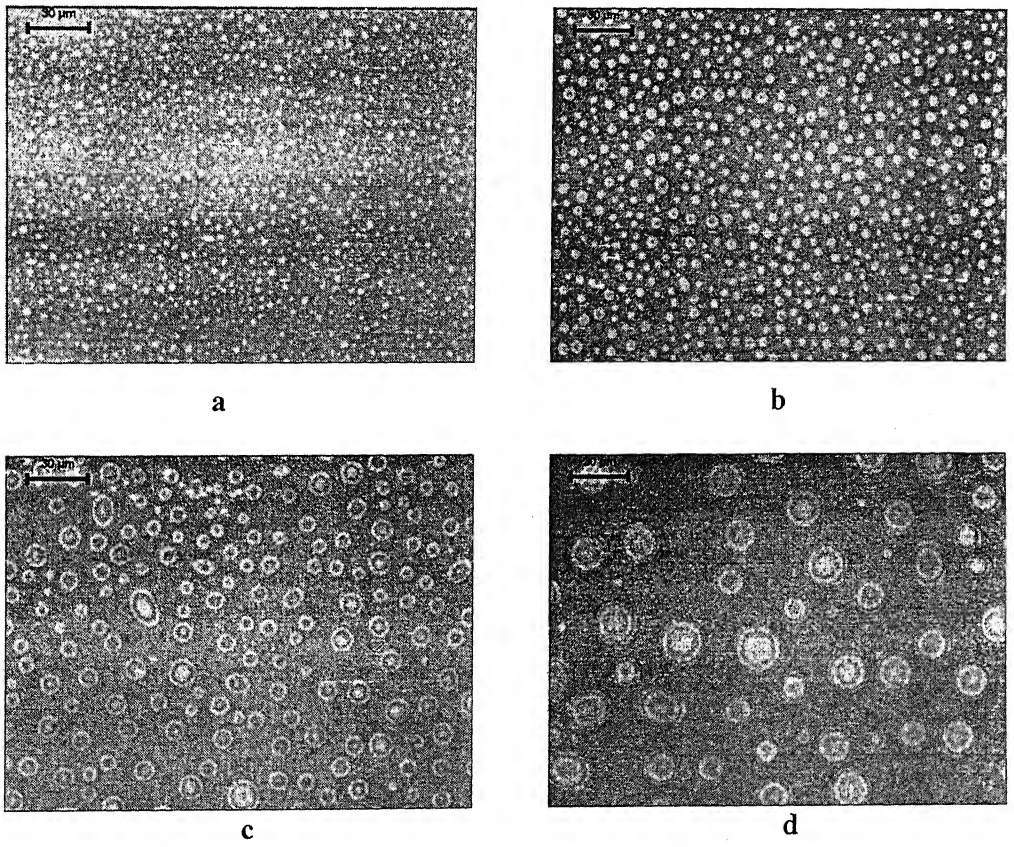

Figure 4.16: Optical micrographs of final dewetted patterns for a 10nm (a), 20nm (b), 30nm (c), and 50nm (d) polystyrene film on Quartz substrate after 6 hours of exposure in saturated solvent (toluene) vapour at 25°C. The bar size is 30 microns for all images. The interference fringes are due to height difference of the polymer droplets.

SUMMARY AND FUTURE STUDY:

We have observed that Dewetting of thin polymer (polystyrene) film on silicon substrate can be induced by solvent vapour. The process can be divided into four distinct stages, (a) Rupture of film through hole formation, (b) hole growth and coalescence to form polygonal "cellular" structure (c) disintegration of polymer ridges forming the polygon into spherical drops due to Rayleigh instability and (d) fingering instability of the hole rims during hole expansion. These fingers again disintegrate into polymer droplets and are predominant for thicker films. We investigated the variation of different characteristic features like initial no of holes per unit are (N_H), Polygon diameter (D_p), Mean equivalent diameter (D_d) of droplets with initial film thickness (h). It is found that $N_H \propto h^P$ where P = -4.9 (for whole data range) or -3.8 (upto 30nm), $D_p \propto h^q$ where q = 2.4788 (for whole data range) or 1.9229 (upto 30nm) and $D_d \propto h^{1.547}$. These values are comparable to the theoretical prediction of Sharma and Reiter [44]. For drop size distribution two dominant drop sizes are found for thicker film (30 and 50nm). This may be due to bimodal dewetting which is dominant for thicker films. Another reason may be due to difference in drop size between drops formed from fingers elongated from hole rims and drops formed during breaking up of polygonal "cellular" structure. The same phenomenon is also observed with thin polymer film coated on Quartz substrate.

However,

1. We are not able to give any experimental proof for decrease of Glass transition temperature (T_g) of polymer film in presence of solvent.

2. The characterization is based on the initial film thickness i.e film thickness prior to exposure in solvent, while ideally the thickness change due to swelling of the film in presence of solvent has to be considered.

Based on this study the dynamics of the process can be investigated. The reason given behind the observations has to be confirmed. The dewetting of a bi-layer film induced by solvent can be investigated.

Bibliography

1. Kajari Kargupta, *Ph. D Thesis, IIT Kanpur*, 2001.
2. G. Reiter, *Phys. Rev. Lett.*, 8, 75, 1992.
3. G. Reiter, *Langmuir*, **9**, 1344, 1993.
4. W. Zhao, M. H. Rafailovich, J. Sokolov, L.J. Fetters et al. *Phys. Rev. Lett.*, **10**, 70, 1993.
5. C. W. Extrand, *Langmuir*, **9**, 447, 1993.
6. G. Narsimhan and E. Ruckenstein, *Langmuir*, **2**, 494, 1986.
7. D. S. H. S. R. Sarma, J. Pandit and K. C. Khillar, *J. of Colloid Interface Science*, **139**, 519, 1990.
8. M. K. Mohanty, H. T. Davis and L. E. Scriven, *Surface Phenomena in Enhanced Oil Recovery.* P 395. Plenum Pub. Co. New Work, 1981.
9. A. Scheludko, *Adv. Colloid and Interface Science*, **14**, 295, 1983.
10. A. Sharma, *Biophys. Chem.*, **47**, 87, 1993.
11. A. Sharma, *J of Dispersion Sci. and Tech.*, **13**, 1495, 1992.
12. A. Sharma, R Khanna and G. Reiter, *Colloid Surf.*, **B 14**, 223, 1993.
13. A. Sharma, E Ruckenstein, *J. Colloid Interface Science*, **111**, 8 1985.
14. Vrij A., Overbeek J. T. G., *J. Am. Chem. Soc.*, **90**, 3074, 1968.
15. Thiele U., Velarde M. G. and Neuffer K., *Phys. Rev. Lett.*, **87**, 016104, 2001.
16. Thiele U., Neuffer K., Pomeau Y. and Velarde M.G., *Colloids Surf. A*, **206**, 135, 2002.
17. Cazabat A. M., *Liquids at interfaces (Les Houches Session series)* ed J. Charvolin, J. F. Joanny and J Zinn-Justin (Amsterdam: Elsevier) 1990.
18. Müller M., MacDowell L. G., Müller-Buschbaum P. Wunnicke O. and Stamm M., *J. Chem. Phys.* **115**, 9960, 2001.
19. Seeman R., Herminghaus S. and Jacobs K. *Phys. Rev. Lett.*, **86**, 5534, 2001.

20. Shinichi Sakurai, Katsunori Tanaka, Shunji Nomura, *Polymer*, **34**(5), 1089, 1993.

21. M. Mertig, U. Thiele, J. Bradt, D. Klemm, W. Pompe, *Appl. Phys. A*, **66**, S565-S568, 1998.

22. N. Samid-Merzel, S. G. Lipson, and D. S. Tannhauser, *Physical Review E*, **57**(3), 2906, 1998.

23. Zravko Mitov and Eugenia Kumacheva, *Phys. Rev. Lett.*, **81**(16), 3427, 1998.

24. Masato Yamamura, Takatoshi Nishio, Toshihisa Kajiwara, Kitaro Adachi, *Chemical Engineering Science*, **57**, 2901-2905, 2002.

25. Robert D. deegan, Olgica Bakajin, Todd F. Dupont, Greb Huber, Sidney R. Nagel & Thomas A. Written, *Nature*, **389**, 827, 1997.

26. Robert D. Deegan, *Physical Review E*, **61**(1), 475, 2000.

27. Adachi E., Dimitrov A. S., Nagayama K., *Langmuir*, **11**, 1057, 1995.

28. Olaf Karthaus, Lars Grasjo, Norihiko Maruyama and Masatsugu Shimomura, *Chaos*, **9**(2), 308, 1999.

29. X. Gu, D. Raghavan, J. F. Douglas, A. Karim, *J. of polymer Science: Part B: Polymer physics*, **40**, 2828, 2002.

30. F. Brocard and J. Daillant, *Can. J. Phys.*, **68**, 1084, 1990.

31. A Sharma and R Khanna, *Phys. Rev. Lett.*, **81**, 3463, 1998.

32. R Konnur *et al., Phys. Rev. Lett.*, 84, 931, 2001.

33. J Koplik and J. R. Banavar, *Phys. Rev. Lett.*, **84**, 4401, 2001.

34. G. Reiter, *Phys. Rev. Lett.*, **68**, 75, 1992.

35. R. Xie *et al., Phys. Rev. Lett.*, **81**, 1251, 1996.

36. K Jacobs *et al., Langmuir*, **14**, 965, 1998.

37. S. Herminghaus *et al., Science*, **282**, 916, 1998.

38. H. I. Kim *et al., Phys. Rev. Lett.*, **82**, 3496, 1999.

39. M. Sferrazza *et al., Phys. Rev. Lett.*, **81**, 5173, 1998.

40. L. Leibler, K. Sekimoto, *Macromolecules*, **26**, 6937, 1993.

41. F. N. Kelly, F. Bueche., *Journal of polymer Science*, L **1961**, 549-556.

42. Denis Morineau *et al.*,*Journal of Chemical Physics*, **117**(19), 8966, 2002.

43. K. Kargupta, A. Sharma and R. Khanna, *Langmuir*, **20**, 244-253, 2004.

44. A. Sharma and G. Reiter, *J. of Colloid and Interfacial Science*, **178**, 383-399, 1996.

45. Peter Müller-Bausbaum, *J. of Phys.: Condensed Matter*, **15**, R1549-R1582, 2003.